### Title

Channel dynamics and habitat development in a meandering, gravel bed river




### Journal

Water Resources Research, 47(4)

### ISSN

0043-1397



### Authors

Harrison, LR
Legleiter, CJ
Wydzga, MA
et al.



### Publication Date

2011-04-01

### DOI

10.1029/2009wr008926

# Channel dynamics and habitat development in a meandering, gravel bed river

L. R. Harrison,[1] C. J. Legleiter,[2] M. A. Wydzga,[3] and T. Dunne[4]

Received 20 November 2009; revised 1 February 2011; accepted 11 February 2011; published 19 April 2011.

[1] We investigated how channel morphology, flow complexity, and habitat characteristics in a meandering gravel bed river evolved over time from a simple, reconfigured initial condition. Using a time series of topographic data, we measured rates of channel migration and morphologic change, documented patterns of sediment storage, and estimated rates of sediment supply. We constructed, calibrated, and validated hydrodynamic models to quantify how the evolving morphology influenced hydraulic conditions, flow complexity, and habitat suitability for Chinook salmon spawning and rearing. For a series of meander bends with constant curvature, similar bank materials, and an identical flow history, sediment supply and bar storage directly influenced channel migration rates. Habitat modeling indicated that the availability of Chinook salmon spawning habitat increased over time, whereas the majority of the reach continues to provide only low- to medium-quality rearing habitat for juvenile salmonids, primarily because of a lack of low-velocity refuge zones. However, other metrics of flow complexity indicate that areas of favorable flow conditions gradually expanded as point bars developed along the inner bank of each bend. These results indicate that although sediment supply can stimulate channel change and diversify river morphology, which acts to promote flow complexity and provide spawning habitat, these sediment-driven morphological changes might not create bioenergetically favorable habitat for juvenile salmonids.

**Citation:** Harrison, L. R., C. J. Legleiter, M. A. Wydzga, and T. Dunne (2011), Channel dynamics and habitat development in a meandering, gravel bed river, *Water Resour. Res.*, *47*, W04513, doi:10.1029/2009WR008926.

## 1. Introduction

[2] River channel dynamics play an important role in creating and maintaining diverse habitat conditions for multiple life stages of aquatic organisms. In a natural state, the interplay between sediment flux and morphologic response creates a range of channel forms, processes, and disturbances that are important for sustaining species diversity [*Ward et al.*, 2002]. The physical heterogeneity inherent in natural channels and floodplains creates and maintains flow and habitat complexity, which has been recognized as being critical for sustaining viable populations of aquatic organisms [*Power*, 1992; *Palmer et al.*, 2000; *Allan*, 2004].

[3] Studies of natural, regulated, and reconfigured channels have emphasized the importance of a freely migrating channel for the development of complex river ecosystems [*Ligon et al.*, 1995; *McBain and Trush*, 1997; *Clear Creek Restoration Team* (*CCRT*), 2000; *Trush et al.*, 2000; *Richards et al.*, 2002; *Stillwater*, 2002]. One management strategy that has emerged from work on dam-impacted rivers involves reengineering meandering channels and floodplains that are scaled to the postdam hydrology [*CCRT*, 2000; *California Department of Water Resources* (*CADWR*), 2005]. The aim has been to initiate or intensify sediment transport and thus sustain geomorphic processes, such as lateral migration and bar building, which are expected to lead to more complex and dynamic river ecosystems. To date, few field studies have quantified the evolution of channel morphology and habitat conditions from an initial reengineered condition, which is critical for predicting the longer-term changes in habitat availability which might result from the imposed conditions of flow and sediment supply.

[4] Changes in flow and the delivery of sediment can result in a range of morphologic adjustments, produced through a number of different mechanisms. In gravel bed streams, these changes often involve the development of alternate bars and pool-riffle sequences [*Wilkinson et al.*, 2008], and several previous studies have examined the effects of changes in channel width [*Repetto et al.*, 2002] and stage-dependent changes in velocity and cross-sectional area [*Keller*, 1971; *MacWilliams et al.*, 2006] on the maintenance of a stable river morphology. In this study, we examined how the flood-driven evolution of channel morphology affects the flow field at ecologically significant low flows. We conducted the study in a reconfigured channel

[1]Earth Research Institute, University of California, Santa Barbara, California, USA.
[2]Department of Geography, University of Wyoming, Laramie, Wyoming, USA.
[3]Civil and Environmental Engineering, California Polytechnic State University, San Luis Obispo, California, USA.
[4]Bren School of Environmental Science, University of California, Santa Barbara, California, USA.


0043-1397/11/2009WR008926

that featured a meandering planform and pool-riffle longitudinal profile with unnaturally low-amplitude cross-sectional asymmetry at the time of its construction. Because this channel already had appreciable curvature, the effects of point bar development were decoupled from those of meander initiation. We were thus able to investigate how bar growth responds to the imposed curvature and pool-riffle geometry. This simple initial form allowed us to focus on understanding how flow and sediment transport in meander bends affect morphologic evolution and habitat formation.

[5] In meandering rivers, channel migration, bar development, and pool scour are linked to habitat development for salmonids across multiple life stages [*Trush et al.*, 2000]. For instance, alluvial river migration involves pool scour and erosion of the outer channel bank [*Dietrich*, 1987]. The scour pool associated with the meander migration process creates favorable holding habitat for adult salmonids and rearing habitat for juveniles [*Trush et al.*, 2000; *Harvey et al.*, 2005]. Channel migration and the development of point bar deposits on the inner bank provide low-velocity rearing habitat for fry and juvenile salmonids [*Trush et al.*, 2000]. Thus, bar growth and lateral channel shifting are expected to directly influence the development and maintenance of salmonid habitat.

[6] A wide body of literature exists on meandering river mechanics, including theoretical approaches [*Ikeda et al.*, 1981; *Johannesson and Parker*, 1989], numerical modeling [*Darby et al.*, 2002; *Chen and Duan*, 2006; *Rinaldi et al.*, 2008], and detailed field studies of flow and sediment transport processes of meandering rivers [*Dietrich et al.*, 1979; *Dietrich and Smith*, 1983, 1984]. Previous studies indicate that meander migration rates are influenced by the channel curvature, which forces high-velocity fluid away from the channel centerline toward the outer bank [*Ikeda et al.*, 1981; *Sun et al.*, 1996]. In curved channels, declining bed shear stress and sediment transport rates along the inner bank cause net sediment deposition and point bar development [*Dietrich and Smith*, 1983]. The point bar in turn influences the flow field around a bend as the bar forces high-velocity fluid toward the outer bank [*Dietrich and Smith*, 1983]. Sediment storage on point bars, in addition to channel curvature, can affect bank erosion rates [*Dunne*, 1988], and it has been hypothesized that topographic steering effects enhance bend migration [*Lancaster and Bras*, 2002]. Therefore, if bar growth does promote meander migration, this feedback mechanism, along with a sediment supply sufficient to enable bar development, should influence river meandering and the development of channel complexity over the long term.

[7] Point bar development has also been found to lead to more complex flow fields across bar-pool sections because of the increased streamwise and cross-stream velocity gradients associated with bar building [*Legleiter et al.*, 2011]. Aquatic organisms often utilize velocity gradients and other complex flow patterns during feeding and resting activities [*Hayes and Jowett*, 1994; *Crowder and Diplas*, 2002; *Hayes et al.*, 2007]. While bar development has ecological importance for salmonids [*Trush et al.*, 2000] and may enhance velocity gradients across bar-pool sections [*Legleiter et al.*, 2011], relatively little is known about how bar growth drives the evolution of both the magnitude and spatial pattern of flow complexity.

[8] Various metrics of habitat quality and flow complexity have been proposed, including the habitat suitability index [*Leclerc et al.*, 1995], the kinetic energy gradient (KEG), vorticity, and hydraulic strain [*Crowder and Diplas*, 2002; *Nestler et al.*, 2008]. These metrics can be used to quantify habitat quality on the basis of flow depth, velocity, and substrate [*Leclerc et al.*, 1995] as well as velocity gradients [*Crowder and Diplas*, 2002; *Nestler et al.*, 2008]. The focus on gradients in the velocity field stems from the proposed importance of a spatially varying flow field in providing areas of fish resting in low-velocity zones that are adjacent to higher-velocity zones utilized for feeding [*Crowder and Diplas*, 2002]. In a study of fish behavior in complex flows, *Liao* [2007] documented the important influence of velocity gradients and vortices on fish behavior and habitat choice. The vorticity metric has been used to identify low-velocity zones along channel margins and in shallow water habitats [*Jacobson et al.*, 2009]. *Jacobson et al.* [2009] observed that migrating adult sturgeon were found disproportionately on the edges of the channel in areas of high energy dissipation, which were defined as zones of fluid shear, flow separation, and turbulence. *Jacobson et al.* [2009] found that the low-velocity refuge zones and shallow water margin habitat used by sturgeon could be mapped spatially using the spatial gradient in velocity. Because vorticity is defined by the spatial gradients in the flow field and identifies areas of low velocity that are adjacent to areas of higher velocity, *Jacobson et al.* [2009] observed that this flow metric could in turn be used to map the sturgeon habitats along the channel margins. In addition, measures of flow turbulence, such as turbulent kinetic energy, have also been found to correlate well with salmonid density [*Smith et al.*, 2006].

[9] *Crowder and Diplas* [2000] proposed that the kinetic energy gradient has the potential to be used in bioenergetic models that incorporate an organism's location and energy expenditure into habitat suitability calculations. The kinetic energy per unit mass multiplied by a drag coefficient and a frontal area provides the drag force exerted on an organism, and *Crowder and Diplas* [2000] reasoned that by using the drag force, one could estimate the power expended by a particular organism moving from one location to another. Flow complexity metrics therefore have the potential to provide insight on how the flow field may influence fish behavior, which is not captured in simple habitat suitability indices [*Crowder and Diplas*, 2000].

[10] In order to examine relationships between channel evolution and habitat development, we investigate how a reconstructed, simplified, meandering river evolves over time in response to flow and sediment supply. We utilize a time series of topographic data to measure morphologic change, channel migration, and net sediment storage that result from flows ranging from bankfull to an approximate 5 year flow event. We then use this information to quantify the extent to which morphologic adjustments drive the development of more complex flow fields and habitat conditions for salmonids across multiple life stages by developing hydrodynamic models to explore the influence of channel evolution on hydraulic complexity and habitat availability. In doing so, we evaluate three specific hypotheses related to channel dynamics and habitat development in meandering, gravel-bedded rivers: (1) sediment storage on developing point bars increases meander migra-

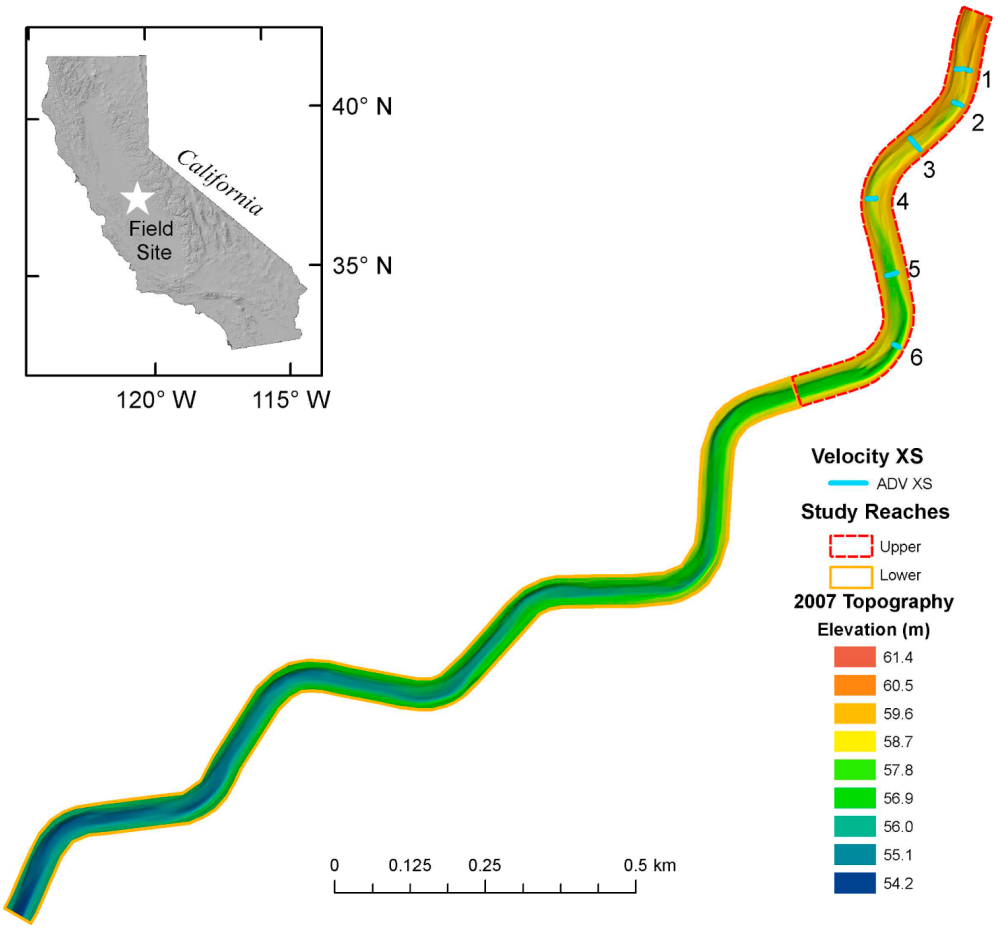


**Figure 1.** Map of the 2.25 km long Robinson Reach on the Merced River, California. Restoration was completed in January 2002 and consisted of grading the floodplain surface and engineering 10 bends with nearly uniform dimensions and channel curvature. The 2007 bed topography of the upper and lower reaches is shown, as well as the cross sections where velocity measurements were made.

tion rates; (2) point bar development leads to more complex flow fields and; (3) morphologic evolution improves salmonid spawning and rearing habitat over time.

## 2. Field Site

[11] The study was conducted in a recently restructured and rescaled reach of the Merced River, California, called the Robinson Reach. The reach represents a field-scale laboratory for investigating the development of channel dynamics and habitat formation from a simple, known initial condition. Our intention is not to evaluate a specific restoration project, nor to assess engineering designs of reconfigured channels. Instead, we focus on the evolution of physical and biological complexity from a simplified state.

[12] The Merced River is a tributary to the San Joaquin River in the Central Valley of California, and at this site drains a watershed of approximately 3305 km$^2$. This study focuses on the Robinson Reach (latitude 37°29′N, longitude 120°28′W) shown in Figure 1, which was reconstructed in January 2002 as part of a larger effort to improve salmon habitat and channel-floodplain functionality that had been degraded by 150 years of placer mining, gravel extraction, and dam construction. The engineered 2.25 km long channel has a single-thread, meandering planform, average bankfull width of 29.2 m, and bankfull discharge of 42.5 m$^3$ s$^{-1}$, which is estimated to have a postdam recurrence interval of approximately 1.5 years. Channel gradient in the upper 0.8 km reach is 0.0025 and decreases in the lower 1.45 km to 0.002 (refer to Table 1 for additional characteristics). The spatially uniform median bed material grain size of 0.052 m was scaled to the postdam bankfull discharge by means of a Shields calculation on the basis of the channel width and cross-sectionally averaged bankfull depth with the expectation that it would be mobilized by discharges occurring every 1–2 years. The channel was designed with shallow riffles and deep pools, with average bankfull widths in the bend axes approximately 7% wider than over the riffles. This aspect of the design differs from field cases, which have reported that riffle reaches are between 12% and 33% wider than pool reaches [*Richards*, 1976; *Carling*, 1991; *Wilkinson et al.*, 2008]. Pools were designed with planar transverse slopes and lacked point bars on the inside of meander bends [*CADWR*, 2005]. The radius of curvature of each bend was set at 71 m (2.4 times the average bankfull width) and the wavelength of each meander at 2010 m (7.2 times the average bankfull width). In the years since construction, sparse, small woody plants have

**Table 1.** Physical Characteristics of the Study Site on the Merced River, California

| Characteristic | Value |
|---|---|
| Bed gradient, upper reach | 0.0025 |
| Bed gradient, lower reach | 0.0020 |
| Bankfull discharge ($m^3$ $s^{-1}$) | 42.5 |
| Mean pool width (m) | 30.3 |
| Mean riffle width (m) | 28.1 |
| Mean bankfull depth (m) | 1.01 |
| $D_{16}$ (mm) | 28.8 |
| $D_{50}$ (mm) | 52.5 |
| $D_{84}$ (mm) | 86.0 |
| Sinuosity | 1.16 |
| Meander wavelength (m) | 2010 |
| Bend apex radius of curvature (m) | 71.4 |

developed along less than 1% of the channel banks and, at present, are too small to exert a significant influence on flow hydraulics and morphologic evolution.

[13] Dams upstream of the project reach dominate the flow hydrograph (Figure 2). A near-bankfull flow release typically occurs each fall and spring, followed by extended periods of base flow, which average 6.4 $m^3$ $s^{-1}$. Two periods of sustained overbank flows have occurred since the channel was constructed. The first flood event occurred during the spring of 2005, when flows remained above bankfull for 81 days and reached a peak of 120.5 $m^3$ $s^{-1}$. The second flood event occurred during the spring of 2006, with a peak discharge of 142 $m^3$ $s^{-1}$ and overbank duration of 119 days (Figure 2). The spring 2005 flow was slightly below the estimated 5 year event of 125.2 $m^3$ $s^{-1}$ (determined from a log Pearson type III analysis calculated from the postdam annual peak flow data for the period from 1967 to 2009), while the spring 2006 flood exceeded the 5 year event.

[14] The sediment supply of the Merced River has been diminished by reservoir construction upstream, and our visual observations have indicated that wash load concentrations are low during bankfull and 5 year floods. However, there is some recruitment of bed material sediment from the bed and banks of the river downstream of the reservoirs.

## 3. Methods

### 3.1. Field Surveys

[15] Following the construction of the channel and floodplain, an "as-built" survey consisting of 25 cross sections along the 2.25 km reach was performed by the *California Department of Water Resources* [2005]. These transects were located in the center of pools and riffles along 10 meander bends, with a mean spacing between cross sections of 30 m (approximately one channel width) and an average distance of 4 m between points along a transect. We completed more detailed surveys of the upper 800 m reach in March 2005, October 2005, and November 2006, as well as a survey of the entire 2.25 km reach in September 2007. The latter topographic data sets encompassed the active channel and roughly 10 m of the floodplain on either bank, with a mean cross-section spacing of 7 m (20% of the channel width) and an average distance of 2 m between points along a transect, although care was taken to measure all significant breaks in slope. Each of these data sets was interpolated to form continuous topographic surfaces using a specialized kriging method for curved channels developed by *Legleiter and Kyriakidis* [2008]. This geostatistical analysis also yielded an estimate of the error variance associated with each bed elevation prediction, and these values were used to estimate the smallest detectable change

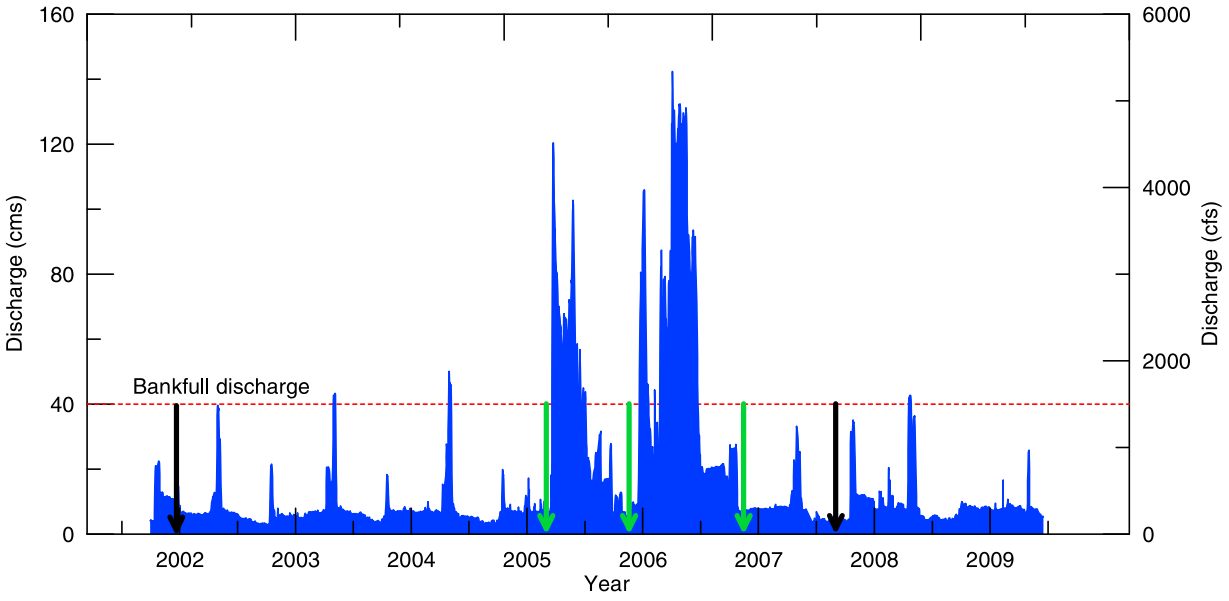


**Figure 2.** Flow discharge on the Merced River at the California Department of Water Resources Snelling gage from 2002 to 2009. The hydrology is regulated by upstream reservoirs, and releases typically include subbankfull flow pulses that occur each fall and spring. Black arrows represent topographic surveys completed on the entire 2.25 km reach in 2002 and 2007. Green arrows indicate the three topographic surveys that were completed on the upper 800 m reach, which effectively bracket the two major flooding events that occurred in spring of 2005 and 2006.

in elevation at each location [*Fuller et al.*, 2003]. For the five survey data sets used in this study, the reach-averaged bed elevation standard errors ranged from 0.06 m for the October 2005 survey to 0.26 m for the sparser, as-built 2002 survey. A reasonable overall estimate of the minimum level of detection for bed elevation change within our study area given the available data is thus on the order of 0.15 m, similar to values reported elsewhere [*Merz et al.*, 2006; *Sawyer et al.*, 2010].

[16] Topographic surveys of the upper 800 m reach conducted in January 2002, March 2005, October 2005, and November 2006 bracket the two flood events and were used to quantify sediment flux and channel change. Given that the survey of the lower reach completed in September 2007 integrates the effects of both floods and a number of bankfull discharge events, we focus primarily on the effects of these two events on channel morphology and habitat availability for the upper 800 m reach. Grain size distributions were measured using traditional pebble counts along bar surfaces and riffles and in pools at a total of 44 sites throughout the upper reach.

[17] To support the development of hydrodynamic models, water surface elevations were measured in the field at discharges of 120.5 $m^3\ s^{-1}$ (~5 year event), 42.5 $m^3\ s^{-1}$ (bankfull flow); 32.6 $m^3\ s^{-1}$ (~75% of the bankfull flow), and 6.4 $m^3\ s^{-1}$ (base flow conditions). Additional hydraulic data included 159 point measurements of velocity collected during a flow of 6.4 $m^3\ s^{-1}$, typical of the spawning-rearing season, along three transects in pools and three in riffles. These data were obtained with an acoustic Doppler velocimeter (ADV), which measured three-dimensional velocities for 60 s at a height above the bed equal to 40% of the local flow depth, approximating the depth-averaged velocity for an assumed logarithmic vertical profile. Velocity fields were also measured in the three pools within the upper reach at bankfull flow with a SonTek acoustic Doppler profiler (ADP), as described in detail by *Legleiter et al.* [2011].

### 3.2. Quantifying Sediment Supply and Storage Change

[18] To quantify how channel morphology has changed as the initially simplified channel evolved, we calculated the sediment supply and spatial patterns of changes in sediment storage for the Robinson Reach. Digital elevation models (DEM) with a 1.0 $m^2$ grid size were developed from the channel surveys for January 2002 (as built), March 2005, October 2005, November 2006, and September 2007. The time periods January 2002 to March 2005, March–October 2005, and October 2005 to November 2006 are referred to in the text as "preflood," "postflood (1)," and "postflood (2)," respectively. The change in bed elevation between successive surveys was calculated at each point in the DEMs. Uncertainties in bed elevation predictions were characterized using the geostatistical techniques described by *Legleiter and Kyriakidis* [2008] and propagated through the elevation difference and sediment storage change calculations following *Fuller et al.* [2003].

[19] The 800 m long upper reach, where almost all the storage change took place, was subdivided into 26 sediment budget cells for the calculation of storage changes in each of the periods defined above. The lateral dimensions of the budget cells varied slightly because of changes in the channel width, while the budget cell length remained constant at 30 m. Within each cell, bed elevation changes were converted to erosion and deposition volumes by multiplying the mean change in bed height by the budget cell area:

$$\Delta V_i = \left(\frac{1}{n_i}\sum_j \left(z_{2,j} - z_{1,j}\right)\right) A_i. \tag{1}$$

These variables are defined as follows: $\Delta V_i$ is net volumetric change ($m^3$) of the $i$th cell, $n_i$ is the number of survey points within the cell, $z_{1,j}$ is bed elevation (m) at time 1 for point $j$ in the DEM, $z_{2,j}$ is bed elevation (m) at time 2 for point $j$ in the DEM, and $A_i$ is the budget cell area ($m^2$) of the $i$th polygon. This calculation yields an event-scale, net measure of erosion or deposition. It should be noted that these storage change calculations are lower bound estimates on the total volumetric change that might have occurred because they do not capture throughput, scour, and fill [*Martin and Church*, 1995; *Ashmore and Church*, 1998; *Church*, 2006] or gravel deflation [*Merz et al.*, 2006; *Sawyer et al.*, 2009].

[20] The total sediment supply to the reach during the study period was calculated using the sediment mass balance equation:

$$I = \Delta S + O, \tag{2}$$

where $I$ is sediment input, $\Delta S$ is change in sediment storage, and $O$ is sediment output. All terms are expressed in units of volume ($m^3$). The cumulative change in sediment storage ($\Delta S$) was calculated for the entire 2.25 km reach between the initial (2002) and most recent (2007) channel surveys. The likelihood of bed load leaving the lower reach (i.e., the sediment output term $O$ in equation (2)) in flows of up to 142 $m^3\ s^{-1}$ was estimated from the Shields criterion:

$$\tau_b^* \equiv \frac{\tau_b}{(\rho_s - \rho)gD}, \tag{3}$$

where $\tau_b$ is the shear stress at the bed of each cell ($N/m^2$), $\rho_s$ is the density of sediment (kg $m^{-3}$), $\rho$ is fluid density (kg $m^{-3}$), $g$ is acceleration due to gravity (m $s^{-2}$), and $D$ (m) is the diameter of the median particle diameter ($D_{50}$). Predicted values of the Shields stress were compared to a critical value of 0.0495 after *Wong and Parker* [2006].

### 3.3. Quantifying Bar Deposition and Bank Erosion

[21] To quantify channel evolution, rates of bank migration and bar deposition were computed. We focused on these processes because of their importance in maintaining dynamic ecosystem functions in meandering rivers [*Trush et al.*, 2000]. Rates of lateral migration were expected to reflect differences in curvature [*Ikeda et al.*, 1981; *Furbish*, 1988; *Johannesson and Parker*, 1989] and in sediment storage on point bars [*Neill*, 1984; *Dunne*, 1988]. Because the Robinson Reach consists of ten bends (Figure 1) with nearly identical radii of curvature (~70 m) that have experienced the same flow history, this site offers an opportunity to explore the relation between sediment storage and bank migration.

[22] Rates of bank migration, averaged over curved reaches, were calculated using surveyed banklines for each successive time period and creating eroded-area polygons following *Micheli et al.* [2004]. Average bank migration distance was calculated as the area of the bank erosion

polygon divided by the length of the polygon's centerline. Our method differed slightly from *Micheli et al.* [2004] in that bank erosion polygons were developed directly from the surveyed banklines for each time period rather than the channel centerlines. Areas of bar deposition were similarly defined by using bed elevation difference maps to digitize polygons indicating where aggradation occurred between surveys on the inner bank of the curved reaches. The bar polygon area was multiplied by the mean change in sediment accumulation and divided by the bar length, yielding a sediment storage volume per unit bar length.

### 3.4. Flow Model

[23] We constructed spatially distributed flow models for the various surveyed morphologies for three purposes. First, we modeled bankfull and overbank discharges up to 142 $m^3$ $s^{-1}$, calibrated using surveyed water surface profiles to understand how the boundary shear stress field adjusts as the bar evolves. At the 2006 peak of 142 $m^3$ $s^{-1}$ overbank flow, the maximum predicted shear stresses were 20% greater than those predicted at bankfull. However, we present only model results for the bankfull stage in this paper because that is the highest discharge for which field measurements were available for validating predicted velocities (section 3.1). Second, we used the flow model to estimate the likelihood of bed material leaving the reach ($O$ in equation (2)) in flows of up to 142 $m^3$ $s^{-1}$. Third, we modeled the low-flow hydraulics during the spawning and rearing seasons to quantify how the evolving morphology influenced hydraulic conditions, flow complexity, and habitat suitability for Chinook salmon.

[24] We utilized the Multidimensional Surface Water Modeling System (MD-SWMS) interface for the Flow and Sediment Transport Morphological Evolution of Channels (FaSTMECH) model developed by the U.S. Geological Survey [*Lisle et al.*, 2000; *Nelson et al.*, 2003; *Barton et al.*, 2005]. Given inputs of discharge, bed topography, and downstream stage, the FaSTMECH computational model predicts the spatial distribution of water surface elevation, flow depth and velocity, and boundary shear stress. The model assumes that the flow is steady and hydrostatic and that turbulence is adequately represented by relating Reynolds stresses to shear via an isotropic eddy viscosity [*Nelson et al.*, 2003]. The eddy viscosity, $K$, comes from an assumed parabolic vertical distribution of eddy viscosity between the bed and the water surface, which results in a logarithmic velocity profile near the bed and a parabolic profile well away from the bed. FaSTMECH solves the full vertically averaged and Reynolds-averaged momentum equations and includes a streamline-based vertical structure submodel that determines the vertical velocity distribution and secondary flows, making it a quasi-3-D model. Calculations of the bed shear stress are made using the quasi-3-D velocity field, with the assumption of a logarithmic velocity relation for the boundary layer, as described by *McLean et al.* [1999]. The governing equations are expressed in a channel-centered orthogonal curvilinear coordinate system, defined by a streamwise axis $s$ oriented along the channel centerline, a cross-stream (normal) axis $n$, and a vertical $z$ axis oriented perpendicular to the bed [*Nelson and Smith*, 1989]. The FaSTMECH model has been tested extensively through detailed laboratory studies [*Nelson et al.*, 1993; *McLean et al.*, 1999; *Maddux et al.*, 2003] and field applications in a variety of rivers [*Andrews and Nelson*, 1989; *Lisle et al.*, 2000; *Barton et al.*, 2005; *May et al.*, 2009].

[25] Two computational grids were used in this study: one for modeling base flow and bankfull hydraulics in the upper reach and another used to model a 5 year overbank flow event over the entire 2.25 km reach. The model grid for the upper reach was approximately 780 m in length and 51 m in width, covering the channel and a strip of floodplain roughly 10 m wide on each bank, with a spacing of 1.0 m in the downstream and cross-stream directions. The model grid developed to simulate overbank flows was 2.25 km in length and covered the entire floodplain width of 675 m, with a spacing of 2.0 m in the streamwise and cross-stream directions.

[26] The lateral eddy viscosity (LEV) parameter used to represent horizontal momentum exchange due to turbulence in eddies and flow separation not generated at the bed was calculated as [*Nelson and McDonald*, 1996]

$$\mathrm{LEV} = 0.01\left(u_{\mathrm{avg}}\right)\left(h_{\mathrm{avg}}\right), \tag{4}$$

where $u_{\mathrm{avg}}$ and $h_{\mathrm{avg}}$ denote reach averages of the depth-averaged velocity and flow depth, respectively. Unlike the eddy viscosity, $K$, used in the vertical submodel, the LEV is an adjustable parameter that can be specified to bring predicted lateral velocity gradients in line with measured flow fields.

[27] Model calibration consisted of comparing measured and modeled water surface elevations and adjusting the flow resistance to minimize the difference between the observed and predicted water surface profiles. FaSTMECH characterizes flow resistance in terms of drag coefficients, $C_d$, which were calculated via a two-step process. First, the drag coefficient was assumed to be spatially constant, and flow resistance was calibrated by determining a single $C_d$ that minimized the root-mean-square error (RMSE) between observed and predicted water surface elevations. The calibrated, constant $C_d$ was then used to perform a second set of model runs in which $C_d$ varied spatially as a function of the local flow depth, using equation (2) of *Legleiter et al.* [2011]. For these runs, we first specified the roughness length as $z_0 = 0.1D_{84}$ [*Whiting and Dietrich*, 1990] using the reach-averaged $D_{84}$ (reported in Table 1) and then used local flow depths from the initial, constant roughness model run to calculate local values of $C_d$ at each node in the computational grid [*McDonald et al.*, 2005].

[28] The model was validated by comparing predicted vertically averaged velocity magnitudes to values measured using an ADV at a discharge of 6.4 $m^3$ $s^{-1}$ at six transects and using an ADP at a bankfull flow at three additional transects, all located in the upper reach of the study site (see Figure 1 for velocity measurement locations). We measured all three components of the velocity field, but the small magnitude of the lateral and vertical components made them unreliable for purposes of validating the model predictions in the field. An assessment of the model sensitivity to the LEV parameter was performed by adjusting the LEV between 50% and 150% of the values calculated from equation (4). Further details regarding model calibration and validation are provided elsewhere [*Legleiter et al.*, 2011].

### 3.5. Hydrodynamic Model Simulations

#### 3.5.1. Modeling Spawning and Rearing Habitat

[29] To investigate how the quantity and quality of habitat adjusted as the bed topography evolved, microhabitat conditions for spawning and juvenile (>60 mm in length) Chinook salmon life stages were modeled at a base flow of 6.4 $m^3$ $s^{-1}$ for each time period. A discharge of 6.4 $m^3$ $s^{-1}$ was selected for these model runs because it is the dam-regulated discharge typically maintained during spawning and rearing seasons for fall-run Chinook and was the target flow specified to maximize Chinook habitat conditions in the constructed Robinson Reach [*U.S. Fish and Wildlife Service* (*USFWS*), 2001; *Gard*, 2006]. We used a commonly applied habitat suitability index approach, based on depth, velocity, and substrate texture [*Leclerc et al.*, 1995], as a means of illustrating the influence of channel evolution on habitat availability.

[30] We used modeled values of depth and velocity and measured bed particle size to calculate dimensionless habitat suitability indices (HSI) $D_{HSI}$, $V_{HSI}$, and $S_{HSI}$, respectively, on the basis of spawning habitat suitability curves developed in the Merced River for fall-run Chinook [*Gard*, 1998, 2006] and juvenile rearing habitat suitability curves developed on the Yuba River [*USFWS*, 2010]. The spawning habitat curves were derived from field observations of mapped redds collected in a 16 km stretch of the Merced River, including the Robinson Reach [*Gard*, 1998], and accounted for both habitat utilization and availability. Juvenile rearing habitat curves were developed on the basis of snorkel surveys in the Yuba River [*USFWS*, 2010]. The Yuba River is the closest river to the Merced in terms of scale (slope and drainage area) within the Central Valley of California for which juvenile rearing HSI curves have been developed.

[31] The global habitat suitability index, $G_{SHSI}$, for spawning ($G_{SHSI} = (D_{HSI})^{1/3}(V_{HSI})^{1/3}(S_{HSI})^{1/3}$) was calculated at each node in the computational grid [*Leclerc et al.*, 1995; *Pasternack et al.*, 2004; *Elkins et al.*, 2007; *Brown and Pasternack*, 2008]. A constant grain size of $D_{50}$ = 0.052 m was used in all calculations. Because nonspawning life stages are less sensitive to the substrate, the $G_{HSI}$ for juvenile rearing habitat quality was calculated as $G_{RHSI} = (D_{HSI})^{1/2}(V_{HSI})^{1/2}$ [*Gard*, 2006].

[32] An important difference between the habitat suitability curves for spawning and rearing life stages is that high-quality spawning habitat is typically located in shallow riffles with optimal spawning velocities between 0.3 and 0.75 m $s^{-1}$ and decreased spawning habitat suitability at depths greater than 0.3 m [*Gard*, 2006]. High-quality rearing habitat tends to be located in pools, with optimal velocities less than approximately 0.4 m $s^{-1}$ and preferred depths greater than 0.75 m [*USFWS*, 2010]. Maps and frequency distributions of the spawning and rearing habitat suitability were developed using the general classes of poor (0–0.1), low (0.1–0.4), medium (0.4–0.7), and high (0.7–1.0) quality habitats [*Leclerc et al.*, 1995].

[33] To assess habitat utilization, the predicted spawning habitat values were compared to the location of redds mapped during fall 2004 [*CADWR*, 2008]. Redds were mapped every 10–14 days during the spawning season, November–December, using a handheld Trimble GeoExplorer GPS with submeter precision. Direct observations of juvenile salmonids in the reach were not available to assess habitat utilization at this life stage.

#### 3.5.2. Flow Complexity Metrics

[34] In addition to preferred depth, velocity, and substrate values at a given location, complex flow patterns, such as velocity gradients, represent another important aspect of fish habitat [*Hayes and Jowett*, 1994; *Crowder and Diplas*, 2002]. Therefore, we also quantified the spatial variability of the flow field for each morphologic configuration in our time series by calculating values of several hydraulic metrics proposed by *Crowder and Diplas* [2000, 2002] and *Nestler et al.* [2008]. The kinetic energy gradient is defined as

$$|\nabla KE| = \sqrt{\hat{i}\left(\frac{\partial}{\partial s}\frac{U^2}{2}\right)^2 + \hat{j}\left(\frac{\partial}{\partial n}\frac{U^2}{2}\right)^2}, \tag{5}$$

where $U$ is depth-averaged velocity magnitude (m/s), $\hat{i}$ and $\hat{j}$ are the unit vectors in the streamwise and cross-stream directions, and $\partial s$ and $\partial n$ are the distance between nodes in the streamwise and cross-stream directions. *Crowder and Diplas* [2000] mapped only the cross-stream ($n$) component of KEG, and *Jacobson et al.* [2009] plotted only the streamwise ($s$) component of KEG, though gradients in kinetic energy are likely to be large in both the streamwise ($s$) and cross-stream ($n$) directions, particularly in curved channels. Therefore, we calculate the absolute magnitude of the complete KEG in the $s$-$n$ coordinate system as defined by equation (5).

[35] The second flow complexity metric was the vorticity, proposed by *Crowder and Diplas* [2006]. For depth-averaged flow, vorticity represents the rate at which each fluid element rotates about its vertical axis:

$$\xi = \hat{k}\left(\frac{\partial v}{\partial s} - \frac{\partial u}{\partial n}\right), \tag{6}$$

where $\xi$ is vorticity ($s^{-1}$); $\hat{k}$ is the unit vector in the vertical direction; and $u$ and $v$ are the depth-averaged velocities in the $s$ and $n$ directions, respectively. *Crowder and Diplas* [2002] proposed that vorticity can be integrated over broader regions of a river channel to calculate the circulation, $\Gamma$, by integrating $\xi$ over a unit area. The expression for circulation is given in discrete form as

$$\Gamma = \sum \xi \Delta A, \tag{7}$$

where $\Gamma$ has units of $m^2$ $s^{-1}$ and $\Delta A$ represents an increment of area ($m^2$). Summation of positive and negative values of vorticity may cancel each other out, thus underrepresenting the true complexity of the region. To overcome this problem, *Crowder and Diplas* [2002] proposed an absolute circulation metric, $\Gamma_{ABS}$, calculated by summing the absolute values of vorticity:

$$\Gamma_{ABS} = \sum |\xi| \Delta A. \tag{8}$$

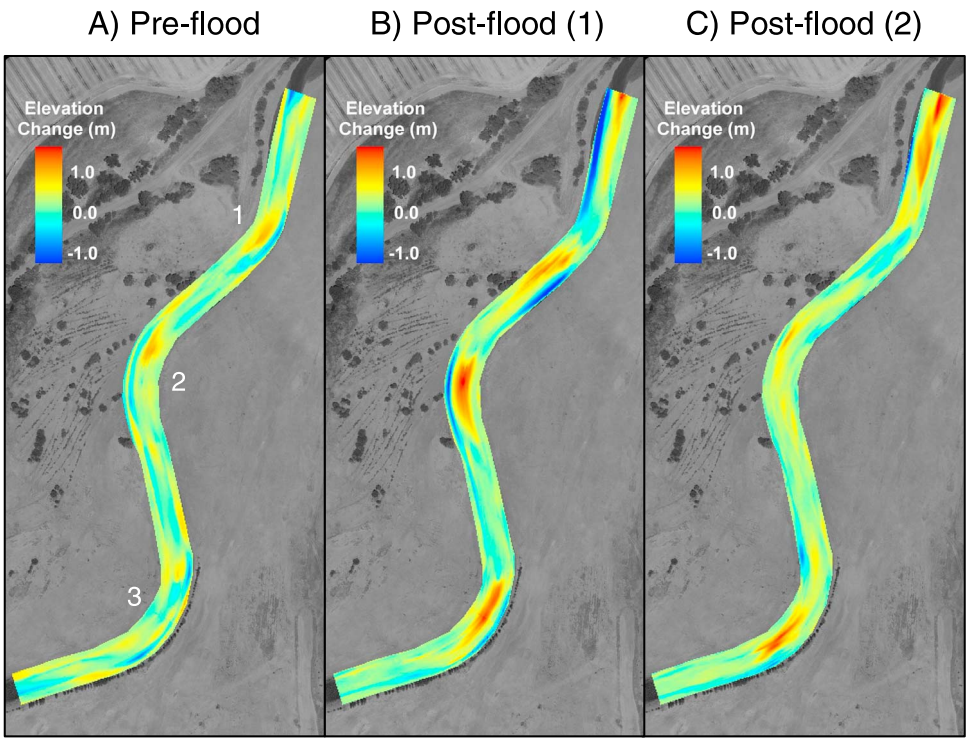


**Figure 3.** Bed elevation differences maps. The successive topographic surveys were completed on (a) January 2002 (as built) to March 2005 (preflood), (b) March–October 2005 (postflood (1)), and (c) October 2005 to November 2006 (postflood (2)). The locations of the three bends in the upper reach are numbered from upstream to downstream.

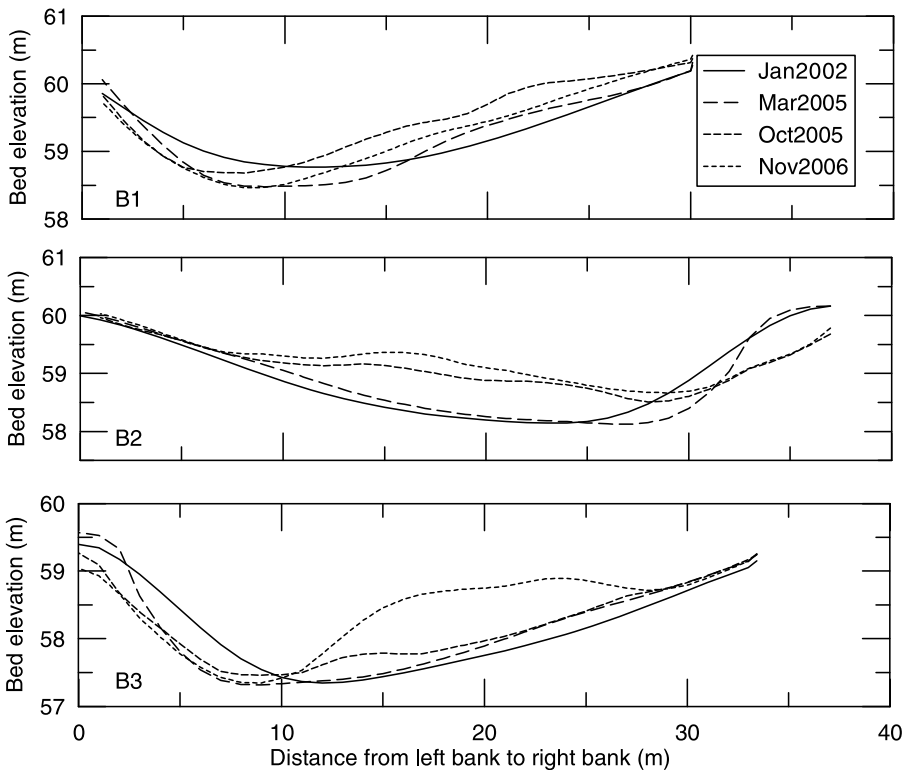


**Figure 4.** Cross-sectional changes in erosion and deposition at bend axes for (top) bend 1, (middle) bend 2, and (bottom) bend 3 of the upper Robinson Reach (January 2002 to November 2006). The initial channel (solid line) was wide and uniform, with a planar transverse slope, and lacked point bars.

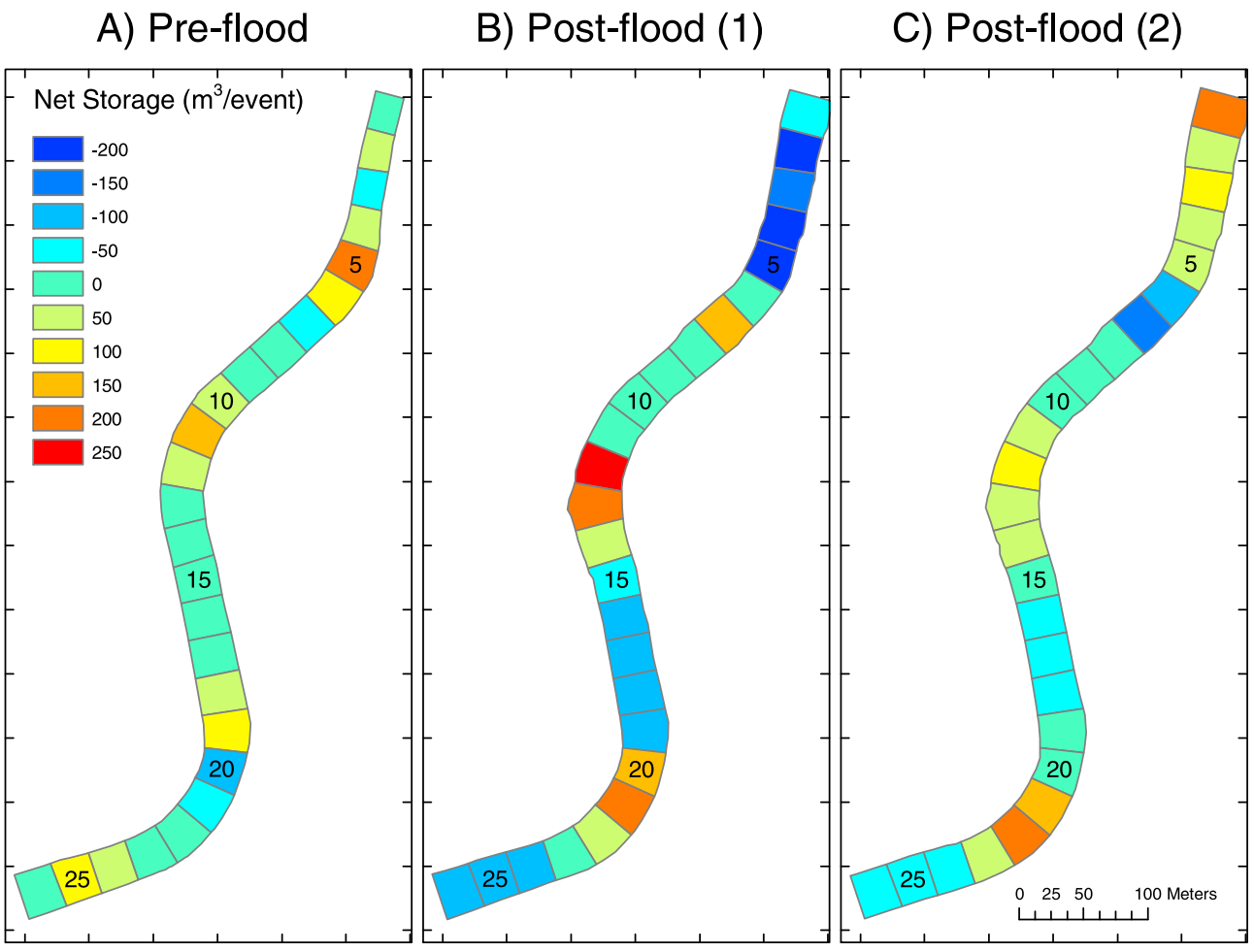


**Figure 5.** Net sediment storage change per runoff event calculated over approximately 30 m × 30 m grid cells. The sediment change calculations illustrate differences in sediment supply and storage within the reach between the three flow periods.

Dividing the absolute circulation over a unit area, the total circulation strength per unit area can be computed as

$$\frac{\Gamma_{ABS}}{A_{TOT}} = \frac{\sum |\xi| \Delta A}{A_{TOT}}, \quad (9)$$

where $\Gamma_{ABS}$ has units of $m^2\ s^{-1}$, $\Delta A$ represents an increment of area (in this case 1 $m^2$), and $A_{TOT}$ is the total wetted area of a reach or morphological unit ($m^2$), yielding units for $\Gamma_{ABS}/A_{TOT}$ of $s^{-1}$.

[36] The hydraulic strain, $S_1$, was initially calculated by *Nestler et al.* [2008] as the summation of the nine spatial derivatives comprising the three-dimensional velocity gradient tensor. Following *Jacobson et al.* [2009], we calculated $S_1$ for the depth-averaged case by summing the absolute values of the four velocity gradients calculated at each point in the *s*-*n* space as

$$S_1 = \left|\frac{\partial u}{\partial s}\right| + \left|\frac{\partial u}{\partial n}\right| + \left|\frac{\partial v}{\partial s}\right| + \left|\frac{\partial v}{\partial n}\right|, \quad (10)$$

where $S_1$ has units of $s^{-1}$. The KEG, vorticity, circulation and $S_1$ metrics were quantified from spatial derivatives calculated between adjacent 1.0 m × 1.0 m model grid cells.

## 4. Results

### 4.1. Sediment Supply

[37] We first established that there was essentially no coarse bed material leaving the reach, meaning that the sediment supply integrated over the period January 2002 to September 2007 was equal to the total change in sediment storage within the reach, which we obtained from our topographic surveys. We estimated the bed mobility by computing the Shields stress in flows up to the peak discharge of 142 $m^3\ s^{-1}$. Comparison of modeled Shields stress values with a critical Shields stress of 0.0495 [*Wong and Parker*, 2006] indicated that only 0.7% and 6% of the channel bed in the lower 1.7 km should be mobile at the bankfull and 5 year events, respectively. These small areas of mobility were predicted to be in riffles, without a continuous zone of sediment transport through the intervening pools. These computations were consistent with our measurements of topographic change for the lower 1.7 km reach, which indicated mean sediment accumulation on bars of 0.25 m between 2002 and 2007 and extensive areas of no

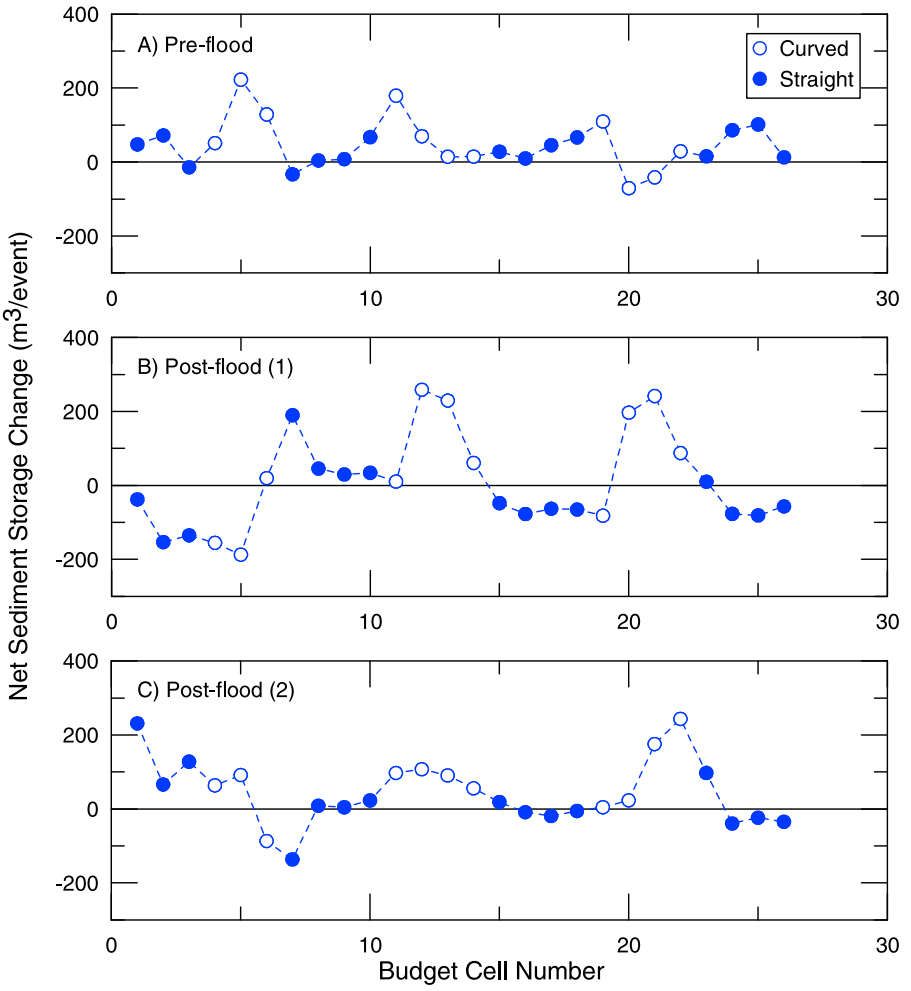


**Figure 6.** Downstream changes in the net sediment storage change for runoff events: (a) early subbankfull flows, (b) first flood, and (c) second flood.

change; our field observations also revealed that the gravel bar surfaces had developed stable structures.

[38] Because bed mobility predictions with the Shields criterion are subject to some degree of uncertainty, we also computed the Shields stresses for the upper reach at the same flows to assess whether they would predict appreciable transport in the regions where we have observed substantial morphologic change. In the upper reach at the same flows, a Shields criterion of 0.0495 predicts continuous zones of bed mobility over 8% and 36% of the bed area for the bankfull and 5 year events, respectively. These results are consistent with our field surveys of topographic change and our observations of loose gravel bar surfaces in the upper reach.

[39] The sediment supply to the reach over the 5 year period, estimated from the total storage change in equation (2), was 2946 ± 50 $m^3$. The mobility calculations and our field observations indicated that this sediment was supplied overwhelmingly by the two 5 year floods, augmented slightly by several bankfull flow events. Dividing the total supply by the mean channel width yields a sediment supply of 100 $m^3\ m^{-1}$ through the upper boundary of the reach over the period 2002–2007.

### 4.2. Channel Evolution

[40] Maps of channel change between the first four surveys (2002–2006) of the upper reach are shown in Figure 3; there was little or no change downstream of the first three bends, and there was no change between the November 2006 and September 2007 topographic surveys. Deposition of up to 1 m on the three point bars accompanied by submeter pool scour (Figure 3a) occurred during the three near-bankfull flows between 2002 and 2005. Bank migration distances, averaged over curved reaches, were highest in the uppermost bend at 1.4 m, compared to 1.0 and 0.7 m for the next two bends downstream.

[41] The sustained high-flow period between March and October 2005 caused more prominent morphologic change than the previous subbankfull to bankfull flows, with point bar growth up to 1.2 m, accompanied by pool scour in excess of 1 m (Figure 4). Average bank erosion in curved reaches during this time period was 1.8, 2.6, and 2.0 m for the first three bends. Bar development continued during the overbank flows between October 2005 and November 2006. Despite the greater magnitude and duration of flooding, pool scour and bank erosion rates were less than in the previous flood (Figures 3b and 3c).

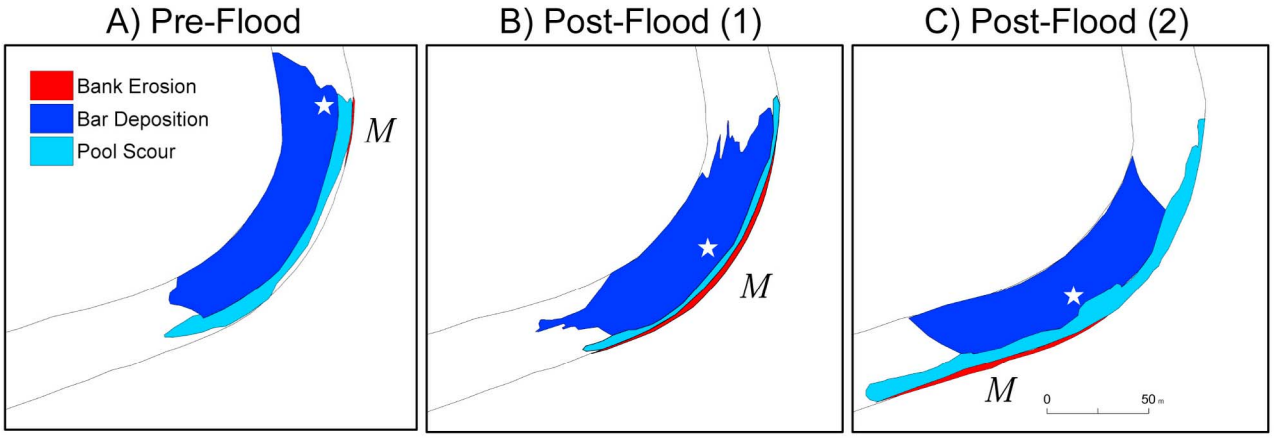


**Figure 7.** Patterns of bank erosion, bar deposition, and pool scour in bend 3. The position of maximum bank migration (*M*) occurs largely in phase with the locus of maximum bar deposition (stars) in the (a) preflood and (b) postflood (1) time periods. The bank migration position advanced through the bend following (c) the second flood, indicating that the bank is migrating faster than the axis of bar deposition.

[42] The early sequence of near-bankfull discharge events (before March 2005) caused minor erosion on riffles (Figure 5a). Over the whole 5 year period, the upper 150 m (budget cells 1–5 in Figure 5) acted as a sediment storage capacitor, as it first accumulated 378 $m^3$, lost 669 $m^3$ of gravel following the first flood, and then gained 580 $m^3$ of sediment following the second flood (Figure 5). The sediment storage changes occurred primarily in the bar-pool sections of the upper reach, with little bed elevation change in the intervening riffles. The location of peak sediment storage change shifted downstream through the reach as a pulse of sediment moved from bar 1 to bar 3 over time (Figure 6).

[43] Figure 7 shows that the position of maximum bank erosion also migrated through the bend over time, with the locus of bank erosion migrating faster than the site of greatest bar deposition. Figure 8 (left) indicates a positive correlation between bar storage and the average migration distance of the outer bank for the upper reach. Changes in both variables were greatest during the first flood, which brought a greater amount of sediment into the upper end of the reach. The relationship between bar deposition and bank migration per unit length of channel between the upper and lower reaches (shown in Figure 1) for the entire study period (2002–2007) is provided in Figure 8 (right). The upper and lower reaches plot as two distinct populations, with bank migration rates greatest in areas of highest bar storage. Channel migration was thus influenced by sediment supply and storage in addition to the initial channel curvature.

### 4.3. Flow Modeling

#### 4.3.1. Model Calibration and Validation

[44] The model was calibrated by adjusting the spatially variable drag coefficient. Inspection of the water surface

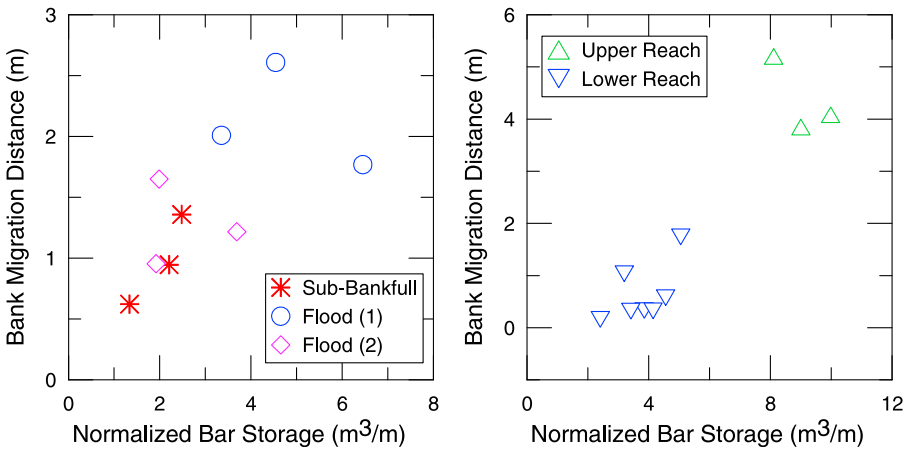


**Figure 8.** Normalized bar storage plotted versus the migration distance of the outer bank. Normalized bar storage is calculated as the measured change in bed elevation between surveys multiplied by the area of deposition and divided by the bar length. (left) Normalized bar storage values versus migration distance for the upper reach between the four channel surveys. (right) Total bar storage and bank migration values for the upper and lower reaches between 2002 and 2007.

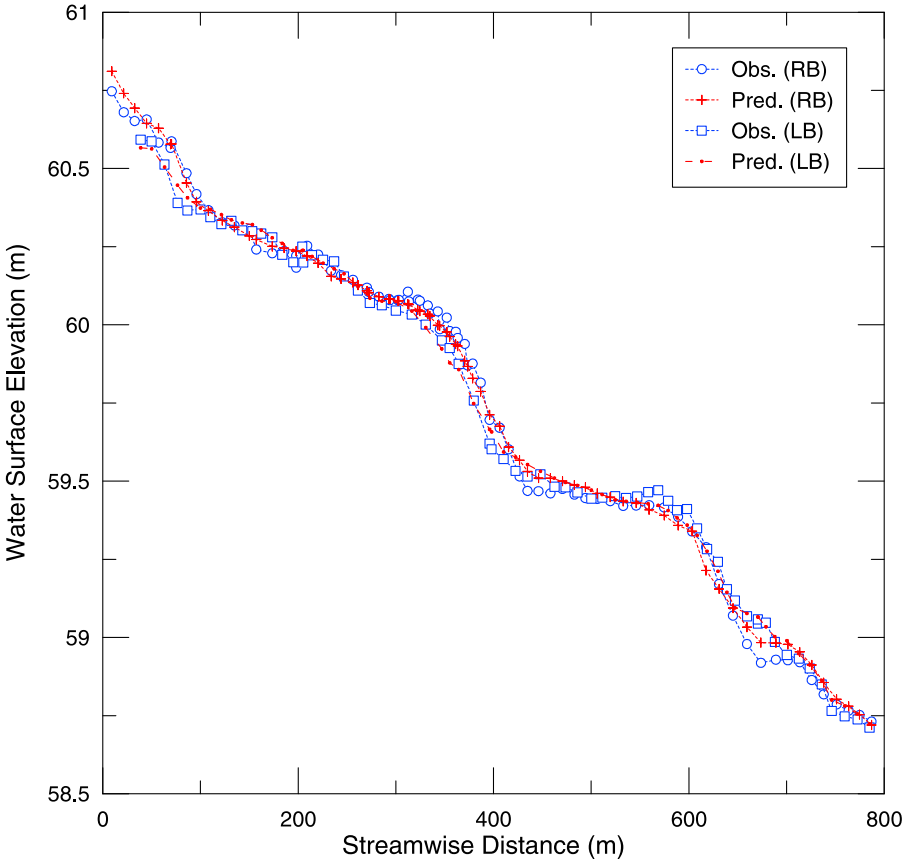


**Figure 9.** Comparison between measured and modeled water surface elevations for a near-bankfull discharge of 32.5 $m^3$ $s^{-1}$. The flow model has also been calibrated with water surface profiles measured at 6.4, 42.5, and 120.5 $m^3$ $s^{-1}$.

elevation (WSE) profile shown in Figure 9 revealed some systematic discrepancies between the calibrated and surveyed profiles, with the model tending to smooth out streamwise variations in the water surface slope. We attribute this modeling error to the abrupt change in width at the entrance and exit of each bend, which might not have been represented accurately in the gridded topography used as input to the flow model. This in turn produced water surface profiles that were smoother than the field data. Nevertheless, overall agreement between modeled and measured WSE values was close, as indicated by the RMSE values in Table 2.

[45] To assess the accuracy of the flow model, predicted vertically averaged velocity magnitudes were compared to measured values at bankfull discharge; results are shown in work by *Legleiter et al.* [2011, Figure 8]. In Figure 10, we show the velocity measurements at six transects at 6.4 $m^3$ $s^{-1}$ because the low-flow simulations were more germane to the habitat characterization in this paper. We did not verify the lateral velocity components directly because their small magnitudes made measurement unreliable, though both the field measurements and model predictions indicated that cross-stream velocities were a small fraction (~10%) of the overall velocity magnitude.

[46] The modeled velocities were not sensitive to the adjusted LEV values, as found by previous workers [*Barton et al.*, 2005]. Regression ($n$ = 118) was used to compare field measurements to predicted velocity magnitudes at a discharge of 6.4 $m^3$ $s^{-1}$ [*Legleiter et al.*, 2011]. These analyses found that the slope of the regression equation was 0.97 and RMSE between predicted and observed velocities was 0.12 m $s^{-1}$ (Table 3); the mean of the measured velocities was 0.59 m $s^{-1}$. Model performance at bankfull flow was also assessed using velocity data recorded by a SonTek ADP. Results from the high-flow regression analyses yielded a slope of the regression equation of 1.34 (Table 3) and an RMSE of 0.27 m $s^{-1}$ (~20% of the mean of the measured velocity of 1.45 m $s^{-1}$) [*Legleiter et al.*, 2011]. Given the close agreement between the observed and predicted velocity magnitudes, computed values of boundary shear stress were assumed to provide accurate estimates of the actual stresses as well.

#### 4.3.2. Modeled Flow Hydraulics

[47] The time series of topographic surveys allowed us to explore how the channel evolution affected the flow

**Table 2.** Calibration Summary for the FaSTMECH Hydrodynamic Model

| Discharge ($m^3$ $s^{-1}$) | $C_d$ | LEV ($m^2$ $s^{-1}$) | WSE RMSE (m) |
|---|---|---|---|
| 6.4 | 0.017 | 0.003 | 0.033 |
| 32.6 | 0.012 | 0.010 | 0.028 |
| 42.5 | 0.010 | 0.012 | 0.042 |
| 120.5 | 0.02 | 0.018 | 0.105 |

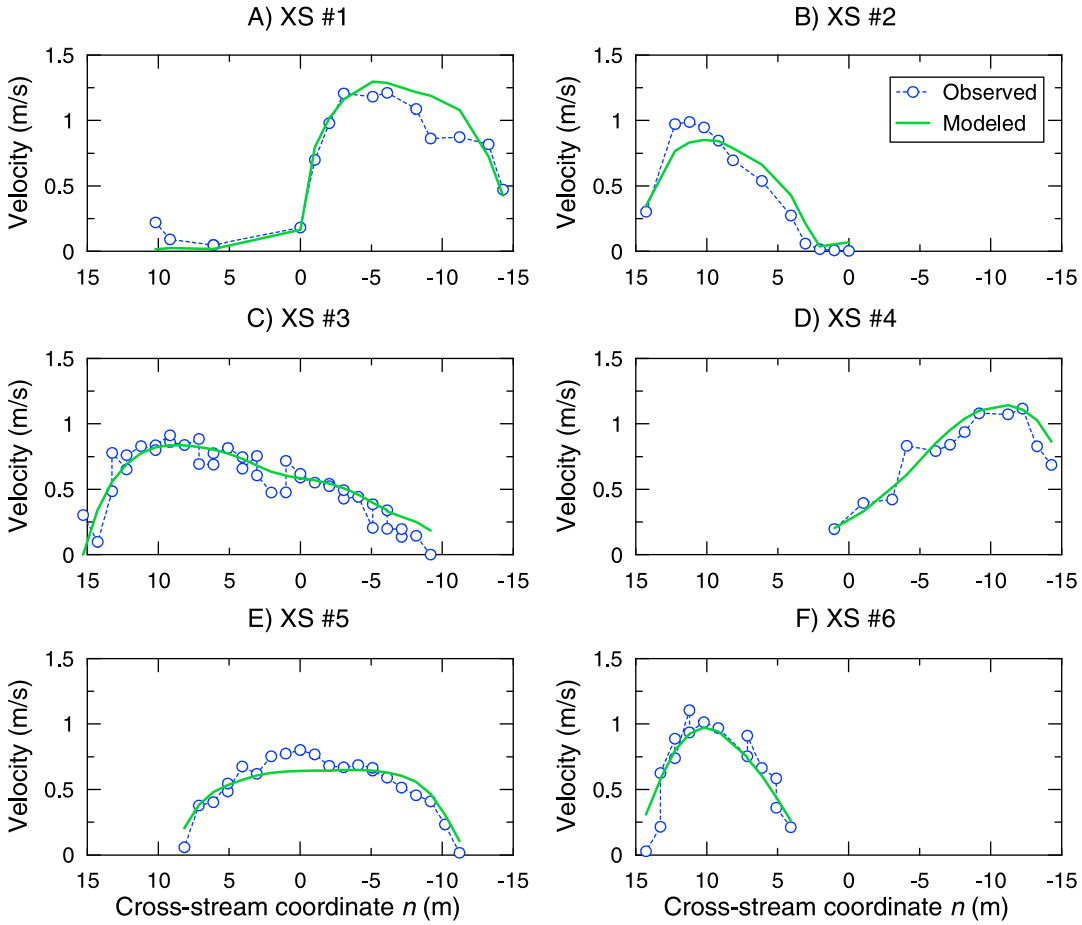


**Figure 10.** Comparison between observed and modeled velocity magnitude for a discharge of 6.4 $m^3 s^{-1}$. View is looking downstream, and the velocity transect location is provided in Figure 1. In general, the predicted and observed velocities are in good agreement. *Legleiter et al.* [2011] provide a velocity comparison at the bankfull discharge.

field. The flow velocities at all discharges were originally greater in the straight riffles than in the curved segments with asymmetric cross-sectional geometries. The morphogenetically significant expression of these effects is seen in the shear stress values (Figure 11) as the value of shear stress maximum increases and its location moves toward the outer bank and shifts downstream beyond the bend apex (Figure 11). In the zone of maximum shear stress, both the downstream and lateral components of the shear stress increase by factors of 2–3. Initially, shear stress values increased in the pool and decreased over the bar surfaces because of shoaling and enhanced drag created by the incipient bar (Figure 12). Subsequent bar and pool aggradation led to increased bed stress across the entire width of the channel (Figure 12). As the bar prograded toward the outer bank (Figure 4) and reduced the cross-sectional area of the flow, a threefold to fourfold increase in the shear stress at the toe of the outer bank occurred.

[48] Changes in base flow hydraulics, representative of flows when adult and juvenile salmonids inhabit the channel, can also be seen as the bed evolves. Initially, velocities are greater over the riffles than the pools (Figure 13). Point bar growth leads to flow constriction, steepening of the water surface gradient, and greater velocities in the pools. Streamwise and cross-stream velocities both increased in pools through time, with the transverse component being approximately 10% of the downstream component. Morphologic changes also led to increased spatial gradients in the streamwise and cross-stream velocities.

#### 4.3.3. Modeled Spawning and Rearing Habitat

[49] Spawning habitat suitability indices were calculated on the basis of point values of flow depth, vertically averaged velocities, and grain size [*Leclerc et al.*, 1995]. Figure 14 indicates that high values of the index used to characterize high-quality spawning habitat were initially limited to riffle crests and the uppermost pool. Following the overbank flows of 2005 and 2006, the higher-quality habitat

**Table 3.** Results From Regression Analyses Comparing Measured and Predicted Velocities Collected at Base Flow and Bankfull Discharges[a]

| $Q$ ($m^3 s^{-1}$) | $b_1$ | $b_0$ (m $s^{-1}$) | $R^2$ |
|---|---|---|---|
| 6.4 | 0.97 | 0.0015 | 0.85 |
| 42.5 | 1.34 | −0.41 | 0.74 |

[a]Linear regression equations were in the form $V_{obs} = b_0 + b_1 (V_{pred})$. The summary statistic listed is the coefficient of determination $R^2$.

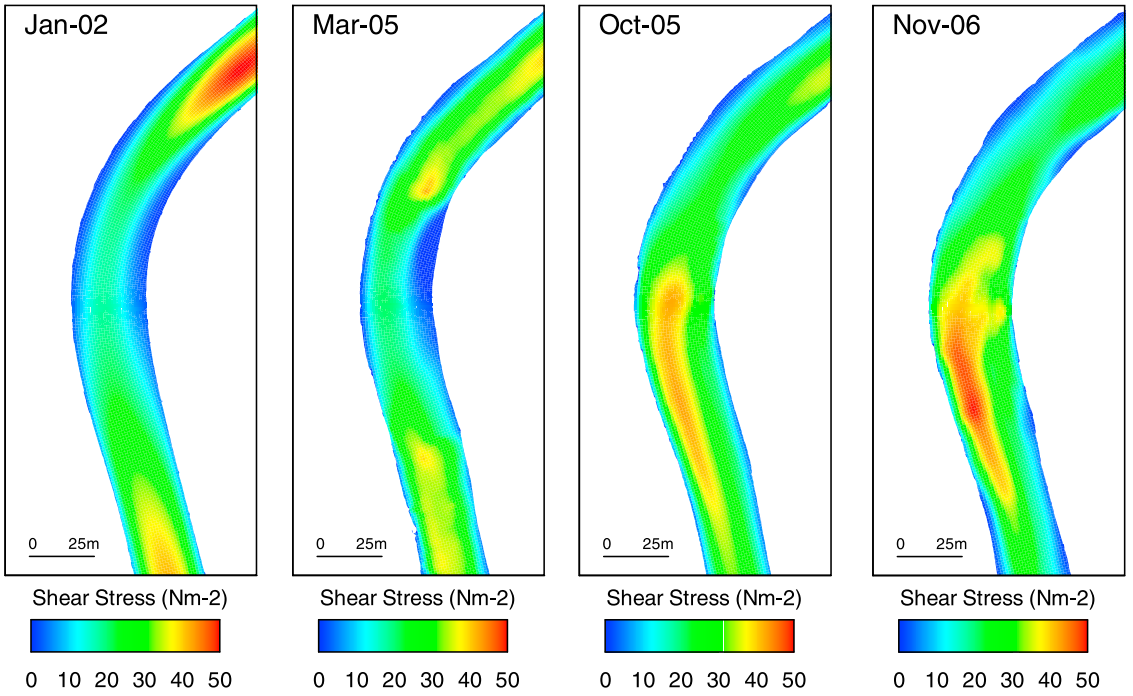


**Figure 11.** Modeled changes in bed shear stress over time at $Q = 42.5$ m$^3$ s$^{-1}$ (bankfull discharge). The developing point bar steers the maximum shear stress toward the outer bank, resulting in both a more pronounced lateral hydraulic gradient and peak stress values located beyond the bend apex. The shift in shear stress maxima through the bend should contribute to maintaining the pool depth at flows capable of transporting sediment.

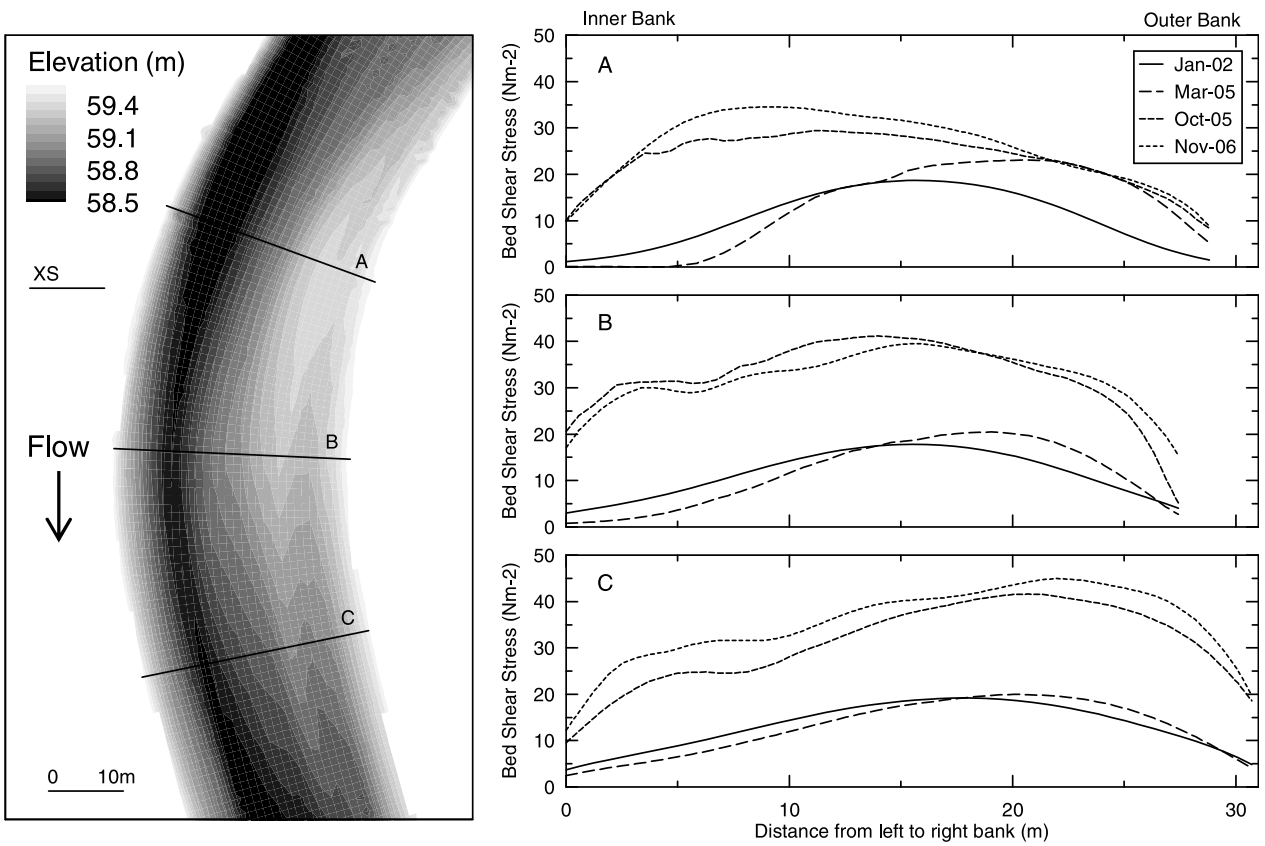


**Figure 12.** Predicted bed shear stress changes over time at $Q = 42.5$ m$^3$ s$^{-1}$ (bankfull discharge) for three cross sections in various parts of the bend. The computed near-bank shear stress shows a threefold to fourfold increase following the enhanced topographic steering effect promoted by point bar development.

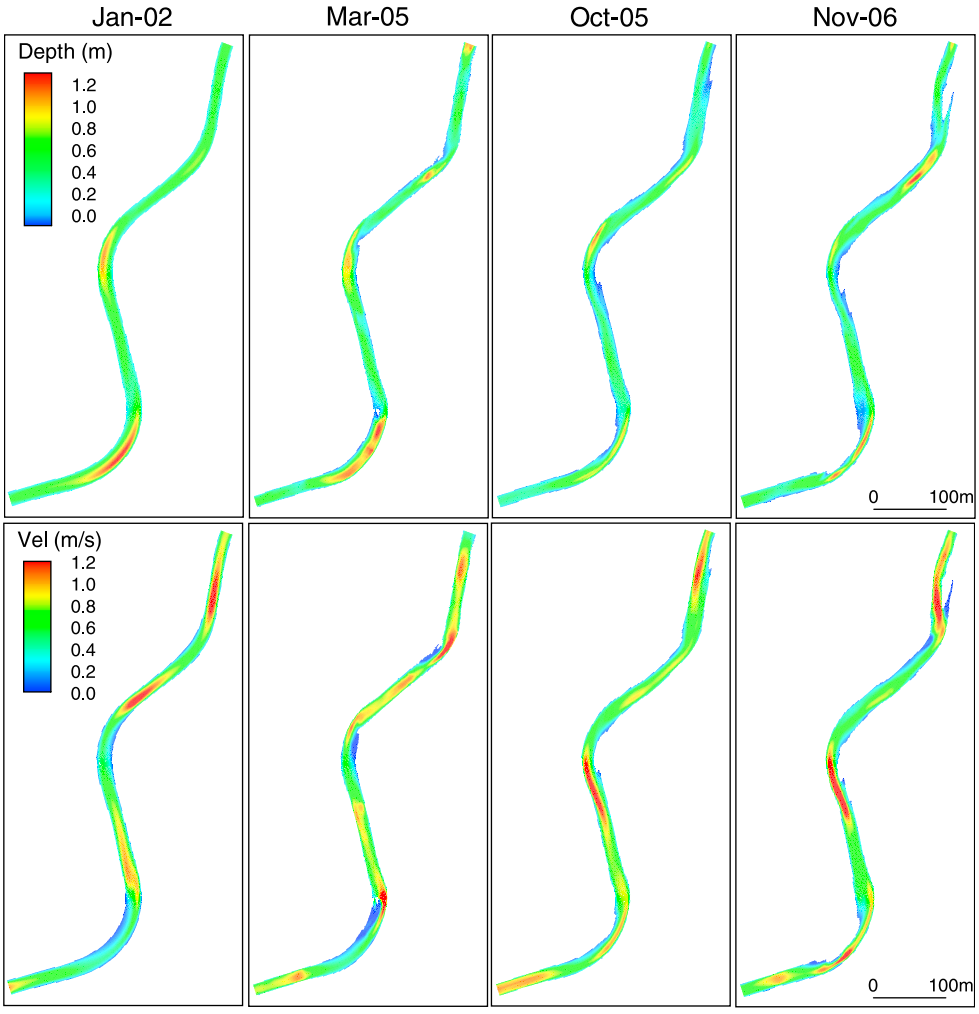


**Figure 13.** (top) Modeled depth and (bottom) vertically averaged velocity for a discharge of 6.4 $m^3$ $s^{-1}$. Computed depths illustrate the development of increased shallow water habitat on channel margins and point bars, while the velocity predictions highlight a shift in the maximum velocity from the riffles to the outer portions of the pools.

gradually expanded throughout the length of the riffles (Figure 14) because of sediment storage and a reduction in the riffle slope. Frequency distributions of the available spawning habitat indicate that medium-high-quality habitat covers more than 90% of the wetted area (Figure 14).

[50] Juvenile Chinook salmon prefer very slow moving, deep water found in pools, channel margins, and off-channel habitats [*Jeffres et al.*, 2008]. Juvenile rearing habitat suitability indices were calculated using point values of flow depth and vertically averaged velocities [*Leclerc et al.*, 1995]. The wide, deep pools initially provided high-quality rearing habitat (Figure 14). Frequency distributions of the juvenile HSI values indicate that medium-high-quality habitat diminishes from 40% to 32% of the wetted area, with the high-quality area diminishing essentially to zero (Figure 15). The decrease in predicted high-quality juvenile habitat is due to the increased velocities found in pools (Figure 13).

#### 4.3.4. Modeled Flow Complexity

[51] In addition to indices based upon point values of depth and velocity, other indices that make use of velocity gradients were used to characterize habitat development. Maps of the absolute magnitude of the kinetic energy gradient, absolute vorticity, and hydraulic strain for the third bend are shown in Figure 16. Each of the three metrics shows a similar pattern, where evolution of the bar-pool morphology increases the magnitude and spatial extent of flow complexity. This is evident in the KEG metric shown in Figure 16, where values in the central portion of the bend were initially 0.02 J $kg^{-1}$ $m^{-1}$ in January 2002 and increased by an order of magnitude to peak values in excess of 0.2 J $kg^{-1}$ $m^{-1}$ by November 2006. Zones of low KEG have remained at the bar head and tail, adjacent to regions with higher KEG that have developed in the pool (Figure 16). Similar increases in absolute vorticity and $S_1$ were observed throughout the reach (Figure 16). Bend-averaged values of the circulation per unit area are provided in Table 4. At the meander bend scale, the circulation per unit area increased by roughly 1.5-fold for the first bend after the first flood event and showed an approximate twofold increase for the second and third bends between 2002 and 2006. A general increase in circulation per unit area has occurred, showing the largest increase between

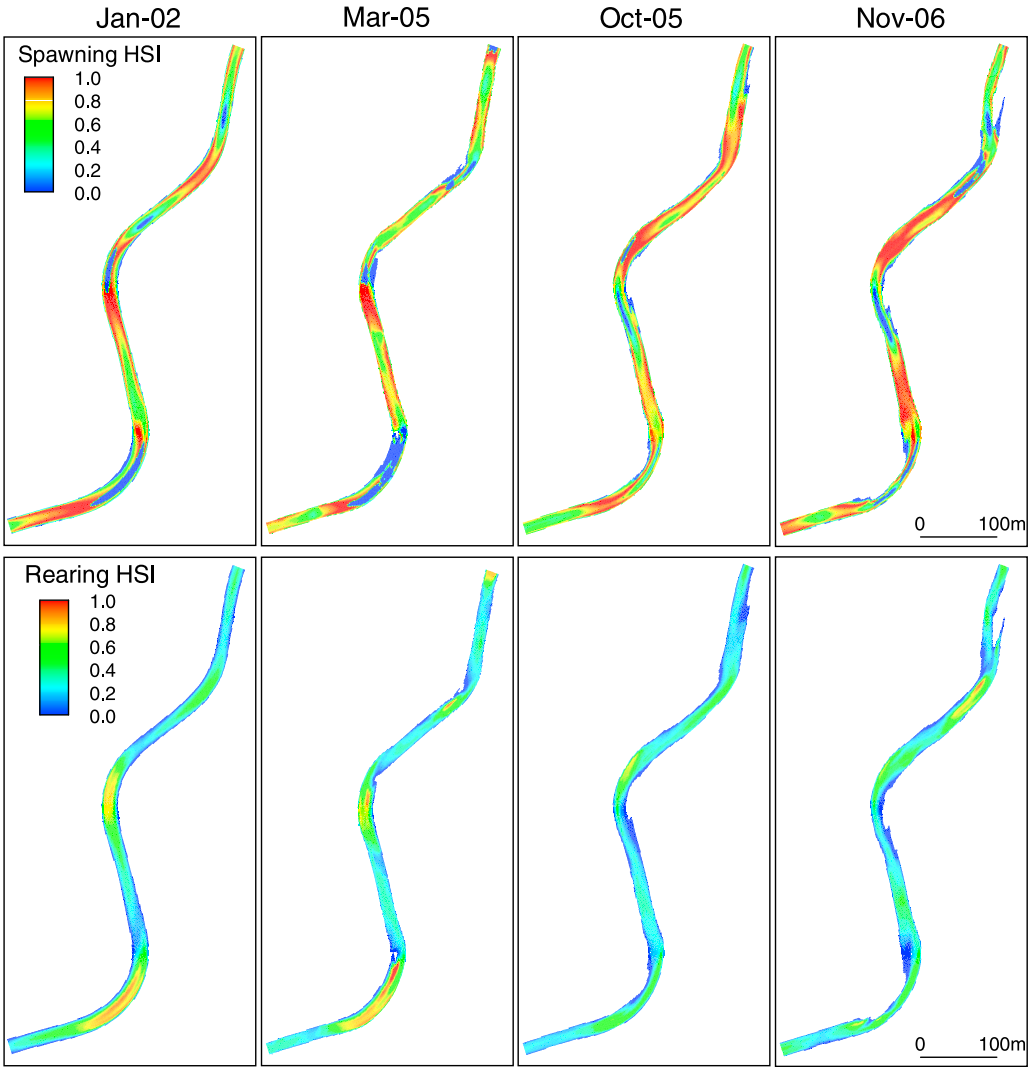


**Figure 14.** Calculated habitat suitability indices (HSI) for (top) fall-run Chinook spawning and (bottom) rearing habitat at a base flow of 6.4 $m^3$ $s^{-1}$. Habitat quality was assessed using the general classes of poor (0–0.1), low (0.1–0.4), medium (0.4–0.7), and high (0.7–1.0) quality habitat [*Leclerc et al.*, 1995].

2002 and 2005 (preflood) and more subtle changes during the following time periods (Table 4).

## 5. Discussion

### 5.1. Channel Dynamics

[52] A frequently stated goal in river restoration projects is to reactivate geomorphic processes in hopes of creating self-maintaining ecosystems. In meandering rivers, the degree to which this objective can be attained will depend in part on the channel's ability to build point bars and scour pools and to migrate laterally across the floodplain. We have studied the earliest stages of the evolution of an engineered, meandering channel as it responded to variations in flow and sediment supply.

[53] Because the initial bankfull width and cross-sectional area were greater in the pools than in the riffles, the flow velocities at all discharges were originally greater in the straight riffles than in the asymmetrical, curved sections, contrary to many natural, low-sinuosity channels that have been interpreted in terms of the velocity reversal [*Keller*, 1971] and flow convergence routing [*MacWilliams et al.*, 2006] hypotheses. The initial construction resulted in a decline in flow velocity from the straight riffles to the curved asymmetrical reaches, causing a reduction of shear stress and deposition of bed material in the curved sections. The sediment deposition occurs on the inner bank, in part because curvature forces flow divergence along the inner bank as the flow is directed toward the outer bank. Second, even the low, initial transverse bed slope generated a topographic steering effect that augmented this routing of flow away from the inner bank [*Legleiter et al.*, 2011]. The growth of the bar and the intensification of the shear stress maximum near the outer bank resulted in the maintenance or lowering of the channel bed elevation near the outer bank, thus creating a pool and a greater transverse slope than the original as-built condition. Bar growth also had the effect of creating narrower pools, in comparison to the riffles; thus,

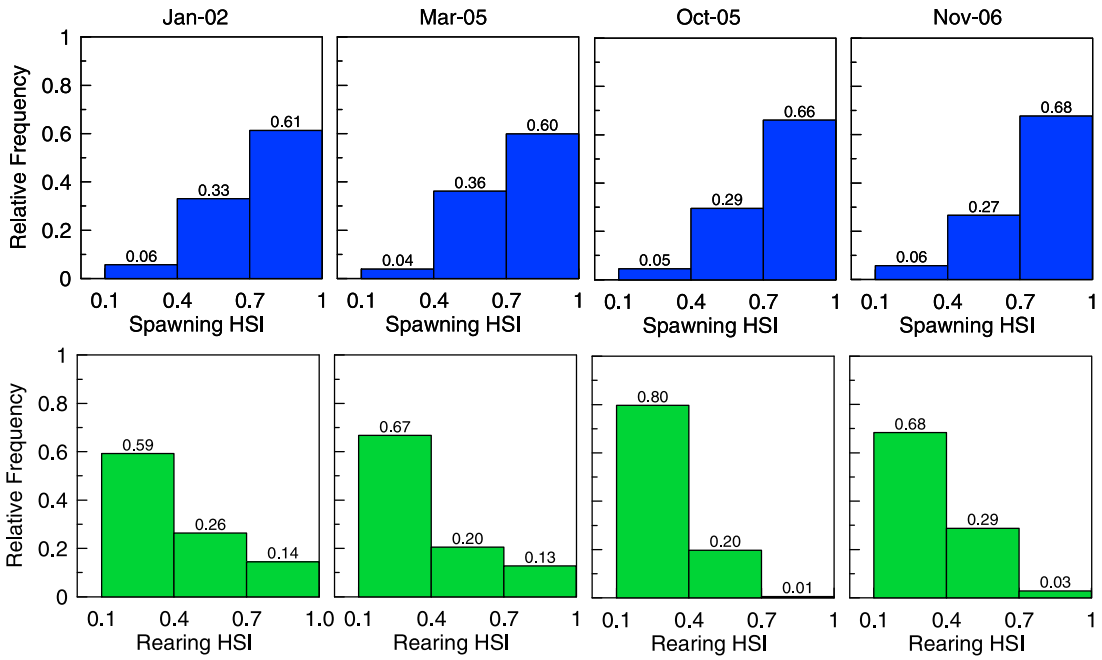


**Figure 15.** Trends in the frequency distributions of the (top) available spawning habitat and (bottom) rearing habitat.

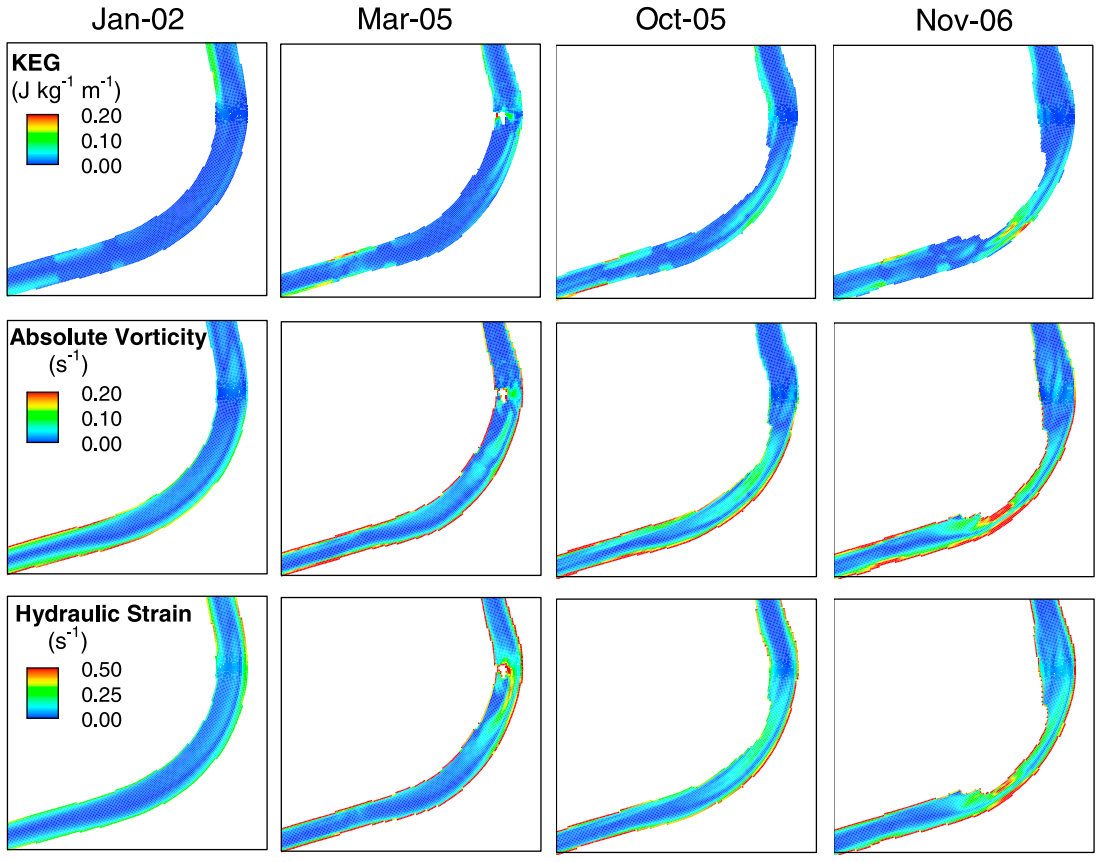


**Figure 16.** Calculated absolute kinetic energy gradient (KEG), absolute vorticity, and hydraulic strain, $S_1$, derived from the flow model output at a discharge of 6.4 $m^3 s^{-1}$. A pronounced increase in the degree of flow complexity is observed with each of the three metrics as the bar-pool morphology develops over time.

**Table 4.** Calculated Bend-Averaged Absolute Circulation[a]

| Date | Bend | Wetted Bend Area ($m^2$) | Absolute Circulation/$A_{TOT}$ ($s^{-1}$) |
|---|---|---|---|
| Jan 2002 | 1 | 2,082 | 0.053 |
| | 2 | 3,193 | 0.027 |
| | 3 | 3,998 | 0.04 |
| Mar 2005 | 1 | 1,660 | 0.123 |
| | 2 | 2,847 | 0.067 |
| | 3 | 3,449 | 0.082 |
| Oct 2005 | 1 | 1,997 | 0.061 |
| | 2 | 3,205 | 0.035 |
| | 3 | 3,215 | 0.074 |
| Nov 2006 | 1 | 2,008 | 0.082 |
| | 2 | 3,110 | 0.055 |
| | 3 | 3,021 | 0.108 |

[a]$Q = 6.4\ m^3\ s^{-1}$.

the width variations shifted phase relative to the bends as a result of the bar-building processes.

[54] The morphologic adjustments resulted in a more asymmetric flow field with a twofold to threefold increase in the shear stress in pools, which enhanced the ability of the channel to maintain the existing pool depth by increasing the flow's capacity to transport sediment through the pool. Sediment transport calculations have not yet been performed for the purpose of evaluating morphologic evolution, but given that bed material transport is a direct, nonlinear function of shear stress, transport rates are expected to be greater for a channel with spatially variable bed stress than for a channel with the same overall dimensions but spatially uniform shear stress [*Lisle et al.*, 2000; *Ferguson*, 2003; *Eaton et al.*, 2006].

[55] Our results indicate that bar growth resulted in greater shear stresses in pools and that rates of bar development and bank migration were positively correlated. This process is consistent with the hypothesis by *Whiting and Dietrich* [1993] that the presence of the bar may enhance bank migration rates both by amplifying the flow velocity near the bank and by increasing the amount of time during which the bank is exposed to the high-velocity flow [*Whiting and Dietrich*, 1993, p. 1101]. Channel migration and bar growth were greatest during periods of prolonged overbank flow when the shear stresses in pools were modeled to be 20% greater than the bankfull values.

[56] Channel migration was influenced by sediment supply and storage in a series of meander bends with constant curvature, similar bank materials, and an identical flow history. If channel curvature alone were the driver of bank erosion, then the bank erosion rates should be close to one another, except for the influence of the small difference in gradient between the upper and lower reach. The discrepancies in bank erosion rates in the upper and lower reaches suggest that bank erosion and lateral migration were driven primarily by point bar deposition.

[57] Our results also suggest that the sediment supply plays an important role in bar development, as suggested by flume studies [*Lisle et al.*, 1993]. Little sediment was supplied to the reach during the subbankfull to bankfull events, but the supply entering the reach was significant for both flood events. Furthermore, the changes that have occurred as a result of the supplied sediment have modified the channel such that any additional sediment delivered to the reach is more likely to be conveyed though the reach as a consequence of the morphologic and hydraulic adjustments that have occurred.

### 5.2. Flow and Habitat Complexity

[58] Habitat modeling indicated that nearly 70% of the upper reach contains high-quality Chinook spawning habitat. This is due to the presence of long riffles in which the water surface gradient and channel bed slope have both decreased over time. Those decreases result from two developments. The first result is that the growth of bars in the curved sections enhanced form drag, which raises the water surface at the lower end of the riffle, decreases the water surface gradient, and induces deposition. At the heads of riffles, scouring results because bar development upstream increases flow velocity and shear stress in the pools, which focuses erosion on the transition from the pool to the riffle. These changes in the water surface and bed profiles diminish the water surface gradient through the riffle, leading to a reduction in flow velocities and thus an increase in the predicted spawning HSI.

[59] In contrast to the high availability of spawning habitat observed at this site, only 32% of the channel was predicted to provide medium-high-quality juvenile habitat (Figure 15). The predicted rearing HSI remains low because of high pool velocities, which result from low flow resistance offered by the pool boundary and steepening of the water surface gradient in curved reaches due to flow constriction by the growing bars. The rearing HSI does not reflect small-scale habitat features such as undercut banks, which are developing slowly in the study reach.

[60] The HSI approach used to quantify habitat is an inherently local habitat measure that is independent of other nodes. The flow complexity metrics, which do account for gradients in velocity, thus can compliment the more simple HSI metrics. The flow metrics calculated in this study indicated that the areas of relatively high KEG, vorticity, and hydraulic strain have expanded from the as-built condition in response to bar development and pool scour (Figure 16). In particular, areas of low flow complexity have remained at the bar head and tail, adjacent to regions with higher flow complexity that have developed in the pool (Figure 16), which should result in improved feeding and resting conditions for salmonids [*Hayes and Jowett*, 1994].

[61] In a straight gravel-bedded reach of the Feather River, located in the Central Valley of California, *Crowder and Diplas* [2002] reported circulation values of 0.045 $s^{-1}$ for a roughly 1000 $m^2$ reach without boulders and 0.054 $s^{-1}$ for the same reach with boulders using a 2-D flow model. The mean circulation value calculated in the bends of the Robinson Reach (Table 4) was 0.04 $s^{-1}$ when the bar amplitude was initially low, and increased to 0.08 $s^{-1}$ because of bar growth. *Shields and Rigby* [2005] calculated circulation values from ADP measurements in bends of a sand-bedded river with radius of curvature to width ratios of 3.4 (gentle bend) and 1.3 (sharp bend) and report values of 0.024 and 0.034 $s^{-1}$ for the gentle and sharp meander bends, respectively. The mean of the circulation values among our three bends, with radius of curvature to width ratios of 2.4, was initially 0.04 $s^{-1}$ and doubled with bar development. Thus, the flow complexity values in the Robinson Reach equaled or exceeded those reported in a sand-bedded meandering channel and a straight gravel-bedded channel.

### 5.3. Implications for River Management

[62] One potential strategy for managing the numerous dam-impacted tributaries that drain the Sacramento and San Joaquin rivers in California's Central Valley involves rescaling channels to the postdam hydrology and attempting to manage for key physical processes and the resulting habitat characteristics. Several of the restoration efforts conducted in this region have been motivated by the goal of enhancing self-sustaining river ecosystems [*McBain and Trush*, 1997; *CALFED Bay-Delta Program*, 2000; *CCRT*, 2000; *Trush et al.*, 2000; *Stillwater*, 2002] through manipulation of channel form, flow conditions, and/or sediment supply. Results from the Robinson Reach indicate that the channel evolved in the manner envisioned by *Trush et al.* [2000], influenced by channel curvature and driven by sediment supply. The establishment of a mobile channel with an adequate supply of bed material initially favors the development of spawning habitat because the bars and riffles that provide such habitat can become more extensive. However, juvenile rearing habitat depends on small-scale morphological features, such as undercut banks, and greater flow resistance than is encountered in simple channels without added structure.

## 6. Conclusions

[63] This study examined how a reconfigured, meandering gravel bed river evolved over time in terms of morphology, flow complexity, and the availability of spawning and rearing habitat. Bar growth and bank erosion were greatest during periods of sustained overbank flow. Comparison between the bar storage and bank migration rates between the upper and lower reaches implies that large changes in sediment storage change are associated with high bank erosion rates, as found by previous workers [*Dunne*, 1988; *Constantine*, 2006]. Model predictions of bed shear stress at bankfull flow indicated that bar development caused a pronounced shift in the maximum shear stress location from the pool center toward the outer bank due to topographic steering [*Legleiter et al.*, 2011]. Furthermore, bar development increased the near-bank stresses threefold to fourfold for bankfull flow events.

[64] Habitat modeling indicated that ~70% of the reach provides high-quality Chinook salmon spawning habitat, whereas the majority of the reach provides low- to medium-quality rearing habitat for juvenile salmonids, primarily due to a lack of low-velocity refuge zones. Despite the generally low quantity of juvenile rearing habitat, modest increases in flow complexity are occurring. Point bar development increased flow complexity metrics that account for velocity gradients, which are bioenergetically favorable for juvenile salmonids [*Hayes and Jowett*, 1994]. Bar growth produced up to a twofold increase in flow circulation, with mean values generally exceeding previously reported circulation values from a straight gravel bed river and a sinuous sand-bedded river.

[65] **Acknowledgments.** We thank David Encinas and Kevin Faulkenberry at the California Department of Water Resources for providing the initial topographic data set. Richard McDonald with the USGS provided valuable input in the application of the FaSTMECH model within MD-SWMS. José Constantine, Matt Meyers, and Clint Olesen helped collect field data. This work was funded by Calfed Bay-Delta Authority Science Program grant U-05SC-058. Jonathan Nelson, Gregory Pasternack, Graham Sander, and an anonymous reviewer provided valuable comments on an earlier version of this paper.

## References

Allan, J. D. (2004), Landscapes and riverscapes: The influence of land use on stream ecosystems, *Annu. Rev. Ecol. Evol. Syst.*, *35*, 257–284, doi:10.1146/annurev.ecolsys.35.120202.110122.

Andrews, E. D., and J. M. Nelson (1989), Topographic response of a bar in the Green River, Utah to variation in discharge, in *River Meandering*, edited by S. Ikeda and G. Parker, *Water Resour. Monogr. Ser.*, vol. 12, pp. 463–485, AGU, Washington, D. C.

Ashmore, P. E., and M. Church (1998), Sediment transport and river morphology: A paradigm for study, in *Gravel-bed Rivers in the Environment*, edited by P. C. Klingeman, et al., pp. 115–148, Water Resour. Publ., Highlands Ranch, Colo.

Barton, G. J., R. R. McDonald, J. M. Nelson, and R. L. Dinehart (2005), Simulation of flow and sediment mobility using a multidimensional flow model for the white sturgeon critical habitat reach, Kootenai River near Bonners Ferry, *U.S. Geol. Surv. Sci. Invest. Rep.*, *2005-5230*.

Brown, R. A., and G. B. Pasternack (2008), Engineered channel controls limiting spawning habitat rehabilitation success on regulated gravel-bed rivers, *Geomorphology*, *97*, 631–654, doi:10.1016/j.geomorph.2007.09.012.

CALFED Bay-Delta Program (2000), Ecosystem restoration program plan: Strategic plan for ecosystem restoration, 75 pp., Sacramento, Calif.

California Department of Water Resources (CADWR) (2005), The Merced River salmon habitat enhancement project: Robinson Reach phase III, 159 pp., San Joaquin District, Fresno, Calif.

California Department of Water Resources (CADWR) (2008), Evaluating the success of spawning habitat enhancement on the Merced River, Robinson Reach, 22 pp., San Joaquin District, Fresno, Calif.

Carling, P. A. (1991), An appraisal of the velocity-reversal hypothesis for stable pool riffle sequences in the River Severn, England, *Earth Surf. Processes Landforms*, *16*, 19–31, doi:10.1002/esp.3290160104.

Clear Creek Restoration Team (CCRT) (2000), Lower Clear Creek floodway rehabilitation project, channel reconstruction, riparian vegetation, and wetland creation design document, 75 pp., McBain and Trush, Graham Mathews, and North State Resour., Redding, Calif.

Chen, D., and J. G. Duan (2006), Modeling width adjustment in meandering channels, *J. Hydrol.*, *321*, 59–76, doi:10.1016/j.jhydrol.2005.07.034.

Church, M. (2006), Bed material transport and the morphology of alluvial river channels, *Annu. Rev. Earth Planet. Sci.*, *34*, 325–354, doi:10.1146/annurev.earth.33.092203.122721.

Constantine, C. R. (2006), Quantifying the connections between flow, bar deposition, and meander migration in large gravel-bed rivers, Ph.D. dissertation, 191 pp., Univ. of Calif., Santa Barbara.

Crowder, D. W., and P. Diplas (2000), Evaluating spatially explicit metrics of stream energy gradients using hydrodynamic model simulations, *Can. J. Fish. Aquat. Sci.*, *57*, 1497–1507, doi:10.1139/cjfas-57-7-1497.

Crowder, D. W., and P. Diplas (2002), Vorticity and circulation: Spatial metrics for evaluating flow complexity in stream habitats, *Can. J. Fish. Aquat. Sci.*, *59*, 633–645, doi:10.1139/f02-037.

Crowder, D. W., and P. Diplas (2006), Applying spatial hydraulic principles to quantify stream habitat, *River Res. Appl.*, *22*, 79–89, doi:10.1002/rra.893.

Darby, S. E., A. M. Alabyan, and M. J. Van de Wiel (2002), Numerical simulation of bank erosion and channel migration in meandering rivers, *Water Resour. Res.*, *38*(9), 1163, doi:10.1029/2001WR000602.

Dietrich, W. E. (1987), Mechanics of flow and sediment transport in river bends, in *River Channels: Environment and Process*, edited by K. S. E. Richards, pp. 179–227, Blackwell, Oxford, U. K.

Dietrich, W. E., and J. D. Smith (1983), Influence of the point bar on flow through curved channels, *Water Resour. Res.*, *19*, 1173–1192, doi:10.1029/WR019i005p01173.

Dietrich, W. E., and J. D. Smith (1984), Bed load transport in a river meander, *Water Resour. Res.*, *20*, 1355–1380, doi:10.1029/WR020i010p01355.

Dietrich, W. E., J. D. Smith, and T. Dunne (1979), Flow and sediment transport in a sand bedded meander, *J. Geol.*, *87*, 305–315, doi:10.1086/628419.

Dunne, T. (1988), Geomorphological contributions to flood-control planning, in *Flood Geomorphology*, edited by V. R. Baker, R. C. Kochel, and P. C. Patton, pp. 421–438, John Wiley, New York.

Eaton, B. C., M. Church, and T. R. H. Davies (2006), A conceptual model for meander initiation in bedload-dominated streams, *Earth Surf. Processes Landforms*, *31*, 875–891, doi:10.1002/esp.1297.

Elkins, E. M., G. B. Pasternack, and J. E. Merz (2007), Use of slope creation for rehabilitating incised, regulated, gravel bed rivers, *Water Resour. Res.*, *43*, W05432, doi:10.1029/2006WR005159.

Ferguson, R. I. (2003), The missing dimension: Effects of lateral variation on 1-D calculations of fluvial bedload transport, *Geomorphology*, *56*, 1–14, doi:10.1016/S0169-555X(03)00042-4.

Fuller, I. C., A. R. G. Large, M. E. Charlton, G. L. Heritage, and D. J. Milan (2003), Reach-scale sediment transfers: An evaluation of two morphological budgeting approaches, *Earth Surf. Processes Landforms*, *28*, 889–903, doi:10.1002/esp.1011.

Furbish, D. J. (1988), River-bend curvature and migration: How are they related?, *Geology*, *16*, 752–755, doi:10.1130/0091-7613(1988)016<0752:RBCAMH>2.3.CO;2.

Gard, M. (1998), Technique for adjusting spawning depth habitat utilization curves for availability, *Rivers*, *6*, 94–102.

Gard, M. (2006), Modeling changes in salmon spawning and rearing habitat associated with river channel restoration, *Int. J. River Basin Manage.*, *4*, 201–211, doi:10.1080/15715124.2006.9635289.

Harvey, B., S. McBain, D. Reiser, L. Rempel, L. S. Sklar, and R. Lave (2005), Key uncertainties in gravel augmentation: Geomorphological and biological research needs for effective river restoration, 99 pp., CALFED Sci. Program, Sacramento, Calif.

Hayes, J., and I. Jowett (1994), Microhabitat models of large drift-feeding brown trout in three New Zealand rivers, *N. Am. J. Fish. Manage.*, *14*, 710–725, doi:10.1577/1548-8675(1994)014<0710:MMOLDF>2.3.CO;2.

Hayes, J. W., N. F. Hughes, and L. H. Kelly (2007), Process-based modelling of invertebrate drift transport, net energy intake and reach carrying capacity for drift-feeding salmonids, *Ecol. Modell.*, *207*, 171–188, doi:10.1016/j.ecolmodel.2007.04.032.

Ikeda, S., G. Parker, and K. Sawai (1981), Bend theory of river meanders. 1. Linear development, *J. Fluid Mech.*, *112*, 363–377, doi:10.1017/S0022112081000451.

Jacobson, R. B., H. E. Johnson, and B. J. Dietsch (2009), Hydrodynamic simulations of physical aquatic habitat availability for pallid sturgeon in the lower Missouri River, at Yankton, South Dakota, Kenslers Bend, Nebraska, Little Sioux, Iowa, and Miami, Missouri, 2006–07, 78 pp., *U.S. Geol. Surv. Sci. Invest. Rep.*, *2009-5058*.

Jeffres, C. A., J. J. Opperman, and P. B. Moyle (2008), Ephemeral floodplain habitats provide best growth conditions for juvenile Chinook salmon in a California river, *Environ. Biol. Fishes*, *83*, 449–458, doi:10.1007/s10641-008-9367-1.

Johannesson, H., and G. Parker (1989), Linear theory of river meanders, in *River Meandering*, *Water Resour. Monogr. Ser.*, vol. 12, edited by S. Ikeda and G. Parker, pp. 181–213, AGU, Washington, D.C.

Keller, E. A. (1971), Areal sorting of bed-load material: Hypothesis of velocity reversal, *Geol. Soc. Am. Bull.*, *82*, 753–756, doi:10.1130/0016-7606(1971)82[753:ASOBMT]2.0.CO;2.

Lancaster, S. T., and R. L. Bras (2002), A simple model of river meandering and its comparison to natural channels, *Hydrol. Processes*, *16*, 1–26, doi:10.1002/hyp.273.

Leclerc, M., A. Boudreault, J. A. Bechara, and G. Corfa (1995), Two-dimensional hydrodynamic modeling: A neglected tool in the instream flow incremental methodology, *Trans. Am. Fish. Soc.*, *124*, 645–662, doi:10.1577/1548-8659(1995)124<0645:TDHMAN>2.3.CO;2.

Legleiter, C. J., and P. C. Kyriakidis (2008), Spatial prediction of river channel topography by kriging, *Earth Surf. Processes Landforms*, *33*, 841–867, doi:10.1002/esp.1579.

Legleiter, C. J., L. R. Harrison, and T. Dunne (2011), Effect of point bar development on the local force balance governing flow in a simple, meandering gravel bed river, *J. Geophys. Res.*, *116*, F01005, doi:10.1029/2010JF001838.

Liao, J. C. (2007), A review of fish swimming mechanics and behaviour in altered flows, *Philos. Trans. R. Soc. B*, *362*, 1973–1993, doi:10.1098/rstb.2007.2082.

Ligon, F. K., W. E. Dietrich, and W. J. Trush (1995), Downstream ecological effects of dams, *BioScience*, *45*, 183–192, doi:10.2307/1312557.

Lisle, T. E., F. Iseya, and H. Ikeda (1993), Response of a channel with alternate bars to a decrease in supply of mixed-size bed load: A flume experiment, *Water Resour. Res.*, *29*, 3623–3629, doi:10.1029/93WR01673.

Lisle, T. E., J. M. Nelson, J. Pitlick, M. A. Madej, and B. L. Barkett (2000), Variability of bed mobility in natural, gravel-bed channels and adjustments to sediment load at local and reach scales, *Water Resour. Res.*, *36*, 3743–3755, doi:10.1029/2000WR900238.

MacWilliams, M. L., J. M. Wheaton, G. B. Pasternack, R. L. Street, and P. K. Kitanidis (2006), Flow convergence routing hypothesis for pool-riffle maintenance in alluvial rivers, *Water Resour. Res.*, *42*, W10427, doi:10.1029/2005WR004391.

Maddux, T. B., J. M. Nelson, and S. R. McLean (2003), Turbulent flow over three-dimensional dunes: 1. Free surface and flow response, *J. Geophys. Res.*, *108*(F1), 6009, doi:10.1029/2003JF000017.

Martin, Y., and M. Church (1995), Bed-material transport estimated from channel surveys: Vedder River, British Columbia, *Earth Surf. Processes Landforms*, *20*, 347–361, doi:10.1002/esp.3290200405.

May, C. L., B. Pryor, T. E. Lisle, and M. Lang (2009), Coupling hydrodynamic modeling and empirical measures of bed mobility to predict the risk of scour and fill of salmon redds in a large regulated river, *Water Resour. Res.*, *45*, W05402, doi:10.1029/2007WR006498.

McBain, S., and W. J. Trush (1997), The fluvial geomorphology of the Tuolumne River: implications for the riverine ecosystem and salmonid restoration, in *Proceedings of the 27th Congress of the International Association of Hydraulic Research*, vol. 2, edited by S. S. Y. Wang and T. Carstens, pp. 569–574, Am Soc. of Civ. Eng., New York.

McDonald, R. R., J. M. Nelson, and J. P. Bennett (2005), Multidimensional surface-water modeling system user's guide, *U.S. Geol. Surv. Techniques Water Resour. Invest. Rep.*, *11-B2*, 156 pp.

McLean, S. R., S. R. Wolfe, and J. M. Nelson (1999), Predicting boundary shear stress and sediment transport over bed forms, *J. Hydraul. Eng.*, *125*, 725–736, doi:10.1061/(ASCE)0733-9429(1999)125:7(725).

Merz, J. E., G. B. Pasternack, and J. M. Wheaton (2006), Sediment budget for salmonid spawning habitat rehabilitation in a regulated river, *Geomorphology*, *76*, 207–228, doi:10.1016/j.geomorph.2005.11.004.

Micheli, E. R., J. W. Kirchner, and E. W. Larsen (2004), Quantifying the effect of riparian forest versus agricultural vegetation on river meander migration rates, Central Sacramento River, California, USA, *River Res. Appl.*, *20*, 537–548, doi:10.1002/rra.756.

Neill, C. R. (1984), Bank erosion vs. bedload transport in a gravel bed river, paper presented at River Meandering, paper presented at Rivers '83, Am. Soc. of Civ. Eng., New York.

Nelson, J. M., and R. R. McDonald (1996), Mechanics and modeling of flow and bed evolution in lateral separation eddies, 69 pp., U.S. Geol. Surv. Grand Canyon Monit. and Res. Cent., Flagstaff, Ariz.

Nelson, J. M., and J. D. Smith (1989), Flow in meandering channels with natural topography, in *River Meandering*, edited by S. Ikeda and G. Parker, *Water Resour. Monogr. Ser.*, vol. 12, pp. 69–102, AGU, Washington, D. C.

Nelson, J. M., S. R. McLean, and S. R. Wolfe (1993), Mean flow and turbulence fields over 2-dimensional bed forms, *Water Resour. Res.*, *29*, 3935–3953, doi:10.1029/93WR01932.

Nelson, J. M., J. P. Bennett, and S. M. Wiele (2003), Flow and sediment transport modeling, in *Tools in Fluvial Geomorphology*, edited by G. M. Kondolf and H. Piegay, pp. 539–576, John Wiley, Chichester, U. K.

Nestler, J. M., R. A. Goodwin, D. L. Smith, J. J. Anderson, and S. Li (2008), Optimum fish passage and guidance designs are based in the hydrogeomorphology of natural rivers, *River Res. Appl.*, *24*, 148–168, doi:10.1002/rra.1056.

Palmer, M. A., C. M. Swan, K. Nelson, P. Silver, and R. Alvestad (2000), Streambed landscapes: Evidence that stream invertebrates respond to the type and spatial arrangement of patches, *Landscape Ecol.*, *15*, 563–576, doi:10.1023/A:1008194130695.

Pasternack, G. B., C. L. Wang, and J. E. Merz (2004), Application of a 2D hydrodynamic model to design of reach-scale spawning gravel replenishment on the Mokelumne River, California, *River Res. Appl.*, *20*, 205–225, doi:10.1002/rra.748.

Power, M. E. (1992), Habitat heterogeneity and the functional significance of fish in river food webs, *Ecology*, *73*, 1675–1688, doi:10.2307/1940019.

Repetto, R., M. Tubino, and C. Paola (2002), Planimetric instability of channels with variable width, *J. Fluid Mech.*, *457*, 79–109, doi:10.1017/S0022112001007595.

Richards, K. S. (1976), Channel width and riffle-pool sequence, *Geol. Soc. Am. Bull.*, *87*, 883–890, doi:10.1130/0016-7606(1976)87<883:CWATRS>2.0.CO;2.

Richards, K., J. Brasington, and F. Hughes (2002), Geomorphic dynamics of floodplains: Ecological implications and a potential modelling strategy, *Freshwater Biol.*, *47*, 559–579, doi:10.1046/j.1365-2427.2002.00920.x.

Rinaldi, M., B. Mengoni, L. Luppi, S. E. Darby, and E. Mosselman (2008), Numerical simulation of hydrodynamics and bank erosion in a river bend, *Water Resour. Res.*, *44*, W09428, doi:10.1029/2008WR007008.

Sawyer, A. M., G. B. Pasternack, J. E. Merz, M. Escobar, and A. E. Senter (2009), Construction constraints for geomorphic-unit rehabilitation on

regulated gravel-bed rivers, *River Res. Appl.*, *25*, 416–437, doi:10.1002/rra.1173.

Sawyer, A. M., G. B. Pasternack, H. J. Moir, and A. A. Fulton (2010), Riffle-pool maintenance and flow convergence routing observed on a large gravel-bed river, *Geomorphology*, *114*, 143–160, doi:10.1016/j.geomorph.2009.06.021.

Shields, F. D., and J. R. Rigby (2005), River habitat quality from river velocities measured using acoustic Doppler current profiler, *Environ. Manage. N. Y.*, *36*, 565–575, doi:10.1007/s00267-004-0292-6.

Smith, D. L., E. L. Brannon, B. Shafii, and M. Odeh (2006), Use of the average and fluctuating velocity components for estimation of volitional rainbow trout density, *Trans. Am. Fish. Soc.*, *135*, 431–441, doi:10.1577/T04-193.1.

Stillwater (2002), Merced River corridor restoration plan, CALFED Bay-Delta Program, Sacramento, Calif.

Sun, T., P. Meakin, T. Jossang, and K. Schwarz (1996), A simulation model for meandering rivers, *Water Resour. Res.*, *32*, 2937–2954, doi:10.1029/96WR00998.

Trush, W. J., S. M. McBain, and L. B. Leopold (2000), Attributes of an alluvial river and their relation to water policy and management, *Proc. Natl. Acad. Sci. U. S. A.*, *97*, 11,858–11,863, doi:10.1073/pnas.97.22.11858.

U.S. Fish and Wildlife Service (USFWS) (2001), Merced River salmon habitat enhancement project and Robinson Reach phase, initial study/environmental assessment, 92 pp., Sacramento, Calif.

U.S. Fish and Wildlife Service (USFWS) (2010), Flow-habitat relationships for juvenile spring/fall-run Chinook salmon and steelhead/rainbow trout rearing in the Yuba River, Sacramento, Calif.

Ward, J. V., K. Tockner, D. B. Arscott, and C. Claret (2002), Riverine landscape diversity, *Freshwater Biol.*, *47*, 517–539, doi:10.1046/j.1365-2427.2002.00893.x.

Whiting, P. J., and W. E. Dietrich (1990), Boundary shear-stress and roughness over mobile alluvial beds, *J. Hydraul. Eng.*, *116*, 1495–1511, doi:10.1061/(ASCE)0733-9429(1990)116:12(1495).

Whiting, P. J., and W. E. Dietrich (1993), Experimental constraints on bar migration through bends: Implications for meander wavelength selection, *Water Resour. Res.*, *29*, 1091–1102, doi:10.1029/92WR02356.

Wilkinson, S. N., I. D. Rutherfurd, and R. J. Keller (2008), An experimental test of whether bar instability contributes to the formation, periodicity and maintenance of pool-riffle sequences, *Earth Surf. Processes Landforms*, *33*, 1742–1756, doi:10.1002/esp.1645.

Wong, M., and G. Parker (2006), Reanalysis and correction of bed-load relation of Meyer-Peter and Müller using their own database, *J. Hydraul. Eng.*, *132*, 1159–1168, doi:10.1061/(ASCE)0733-9429(2006)132:11(1159).

T. Dunne, Bren School of Environmental Science, University of California, Santa Barbara, CA 93106, USA.

L. R. Harrison, Earth Research Institute, University of California, Santa Barbara, CA 93106, USA. (lharrison@bren.ucsb.edu)

C. J. Legleiter, Department of Geography, University of Wyoming, Laramie, WY 82071, USA.

M. A. Wydzga, Civil and Environmental Engineering, California Polytechnic State University, San Luis Obispo, CA 93407, USA.